Metamorphic constraints on the character and displacement of the South Tibetan fault system, central Bhutanese Himalaya

F.J. Cooper[1], K.V. Hodges[1], and B.A. Adams[1]

[1]*School of Earth and Space Exploration, Arizona State University, Tempe, Arizona 85287, USA*

ABSTRACT

The South Tibetan fault system (STFS), a family of primarily extensional faults that separates the metamorphic core of the Himalaya (expressed as the Greater Himalayan sequence (GHS)) from overlying, predominately unmetamorphosed Tibetan sedimentary sequence (TSS) units, has been mapped for over 2,000 km coincident with the Himalayan range crest. In most areas, the immediate hanging wall of the STFS sole detachment consists of predominately carbonate rocks of lower Paleozoic age. However, in the Bhutan sector of the eastern Himalaya (ca. 89–92°E), the hanging wall of the sole structure is instead frequently mapped at the base of a metamorphosed, predominately siliciclastic succession (the Chekha Formation), and the base of the overlying predominately carbonate rocks (Pele La and Tang Chu Groups) is mapped as a less significant splay of the STFS. Unfortunately, poor exposures throughout central Bhutan make mapping and structural interpretation of these important contacts difficult, resulting in many disparities among geologic maps made by different research groups. The STFS in other parts of the Himalaya accommodates a significant metamorphic discontinuity that should also be apparent in Bhutan. Therefore, as an alternative approach, we have used the Raman spectroscopy on carbonaceous material (RSCM) thermometer to evaluate the evidence for a metamorphic discontinuity across both putative STFS structures.

RSCM thermometric data from 17 samples across three purported STFS klippen in central Bhutan (the Dang Chu, Ura, and Zhemgang klippen) suggest that the contact between the Chekha Formation and the underlying GHS is not a fault with large, postmetamorphic displacement. We find no resolvable change in peak metamorphic temperature across the contact, with a consistent temperature of ca. 560°C, but we see a 130–140°C drop in paleotemperature across the higher contact between the Chekha Formation and overlying Pele La and Tang Chu groups. This change coincides with a major change in structural style, from high-strain, leucogranite-bearing rocks below to large-scale recumbently folded marbles above. Together, the change in deformational character and metamorphic grade suggest that the principal STFS detachment in Bhutan is the structural boundary of the Chekha Formation and the predominantly carbonate rocks above. The presence of an STFS detachment approximately 80 km south of the main STFS fault trace at the crest of the Himalaya, with no match between correlative footwall and hanging wall units along the direction of fault motion implies large displacements on the STFS in the eastern Himalaya.

Keywords: Himalaya; extension; Raman spectroscopy of carbonaceous material; geothermobarometry

INTRODUCTION

Over the past few decades the eastern Himalayan Kingdom of Bhutan has become increasingly accessible to foreign visitors, resulting in a flurry of geologic research that has added critical new information to our understanding of the Himalayan-Tibetan orogenic system (Carosi et al., 2006; Chakungal et al., 2010; Chambers et al., 2011; Cooper et al., in press; Corrie et al., 2012; Daniel et al., 2003; Davidson et al., 1997; Edwards et al., 1999; Edwards and Harrison, 1997; Gansser, 1983; Grujic et al., 2006; Grujic et al., 2002; Grujic et al., 2011; Hughes et al., 2011; Kellett et al., 2009; Kellett et al., 2010; Kellett and Grujic, 2012; Long and McQuarrie, 2010; Long et al., 2011a; Long et al., 2011b; Long et al., 2011c; Stüwe and Foster, 2001; Swapp and Hollister, 1991; Tobgay et al., 2012). However, research progress has been hindered by the dense vegetation and shortage of roads (and, in turn, road-cut outcrops) throughout most of the country. Only in the areas near the Tibetan border are outcrops sufficient to tightly constrain geologic mapping. As a result, there are still many disparities among geologic maps of Bhutan made by different research groups. One outstanding issue regards the position, character, and displacement of the principal basal (or "sole") detachment of the South Tibetan fault system (STFS), a family of primarily extensional faults that crops out for over 2,000 km along the length of the Himalayan range crest (Burchfiel et al., 1992; Burg and Chen, 1984; Hodges et al., 1992; Pognante and Benna, 1993; Searle et al., 1997; Searle, 1999).

Basal low-angle detachments of this system typically mark a metamorphic discontinuity between high-grade metamorphic gneisses and anatexites of the Himalayan core below and lower-grade or unmetamorphosed strata above (Burchfiel et al., 1992). Recent mapping in the central Bhutan Himalaya (Figures 1 and 2) suggests that there may be multiple detachments of the South Tibetan fault system there (e.g. Carosi et al., 2006; Edwards and Harrison, 1997;

63 Grujic et al., 2006; Grujic et al., 2002; Grujic et al., 2011; Kellett et al., 2009; Kellett et al., 2010;
64 Kellett and Grujic, 2012; Long and McQuarrie, 2010; Long et al., 2011a; Long et al., 2011c), an
65 observation similar to that made in several other parts of the orogen where structurally higher
66 detachments are typically marked by tectonite fabrics but not by significant metamorphic
67 discontinuities (Burchfiel et al., 1992; Hodges et al., 1994; Hodges et al., 1996; Searle and
68 Godin, 2003; Searle, 1999).

69 The role of the extensional STFS in the development of the Himalayan orogen is a matter of
70 active debate, largely because constraining the magnitude of its displacement has proved
71 difficult. Generally exposed along the Himalayan range crest, down-dip exposures of STFS
72 detachments that allow direct measurements of minimum displacement are rare. In a recent study
73 in NW Bhutan, Cooper et al. (in press) traced the STFS from the range crest south for ca. 65 km,
74 suggesting large displacements on the system. The presence of STFS detachments even farther
75 south in central Bhutan suggests that minimum displacements on the STFS could be even larger.
76 Grujic et al. (2011), for example, map the STFS ca. 100 km south of the range crest (Figure 2b).
77 Alternatively, mapping by Long and McQuarrie (2010) implies that the breakaway zone for the
78 STFS is present in southern Bhutan. The structural offset between this breakaway and hanging
79 wall units to the north is at most 20 km suggesting limited slip on the STFS.

80 The differences in mapping and interpretation of the STFS in central Bhutan suggests that
81 further work is needed in order constrain the position and thus the significance of the system
82 there. Due to the poor exposures in Bhutan, which have hindered mapping of STFS structures
83 thus far, we have used the widely-applicable Raman spectroscopy on carbonaceous material
84 (RSCM) thermometer to evaluate the evidence for metamorphic discontinuities across the
85 putative STFS structures mapped by previous workers.

STRUCTURAL SETTING

The Himalayan-Tibetan orogenic system

The Himalayan-Tibetan orogenic system is one of our planet's most spectacular signatures of continent-continent collision. Thought to have initiated in the Early Eocene with the closure of the neo-Tethys Ocean (de Sigoyer et al., 2000; Guillot et al., 2008; Leech et al., 2005; Rowley, 1996), collision of the Indian and Eurasian plates created both the highest mountain range and the most expansive area of regional uplift on Earth: the Tibetan Plateau. The Himalayan sector of the orogenic system comprises four broad lithotectonic belts of contrasting metamorphic grade separated by a series of north-dipping faults (Gansser, 1964; Heim and Gansser, 1939; Hodges, 2000; Le Fort, 1975). From south to north, these are the Subhimalayan zone, Lesser Himalayan zone, Greater Himalayan zone, and Tibetan zone. Each of these zones comprises a distinctive package of rocks known as the Eocene to Lower Miocene Rawalpindi and Lower Miocene to Pleistocene Siwalik Groups of the Subhimalayan zone, the Proterozoic to Middle(?) Miocene Lesser Himalayan sequence (LHS), the Neoproterozoic to Ordovician Greater Himalayan sequence (GHS), and the Paleozoic to Eocene Tibetan sedimentary sequence (TSS) (Acharyya and Sastry, 1979; Brasier and Singh, 1987; Brookfield, 1993; Burbank et al., 1997; Critelli and Garzanti, 1994; DeCelles et al., 1998; Gaetani and Garzanti, 1991; Gansser, 1983; Hodges, 2000; Najman et al., 1993; Najman et al., 1997; Parrish and Hodges, 1996; Singh et al., 1999; Stöcklin, 1980; Valdiya, 1980). Rocks of the Subhimalaya, LHS, and GHS are separated by orogen-parallel contractional structures of the Main Boundary thrust system (MBTS) and the Main Central thrust system (MCTS). In the Bhutanese Himalaya, an out-of-sequence thrust fault (the Kakhtang thrust) mapped by Gansser (1983) has been interpreted to have roughly doubled the

thickness of the GHS (Davidson et al., 1997; Grujic et al., 2002) (Figure 1), although the location, age and displacement across this structure are poorly constrained. In contrast to its southern and lower boundary, the top of the GHS is bounded by extensional faults and shear zones of the STFS. The opposing-sense STFS and MCTS are both thought to have been active during the Miocene (Hodges et al., 1992; Hodges et al., 1996; Hubbard and Harrison, 1989; Searle and Rex, 1989), implying that the STFS played an important role in exhuming the GHS metamorphic core.

The structurally highest and northernmost zone is represented by the Tibetan sedimentary sequence (TSS), which generally crops out north of the Himalayan range crest. The TSS comprises low-grade to unmetamorphosed sediments deposited on the northern passive continental margin of India (Gaetani and Garzanti, 1991). Although it is generally accepted that the GHS and the TSS are separated by the STFS throughout most of the Himalaya, the relationships are more controversial in regions south of the range crest where the TSS occurs in a series of low-elevation outliers above GHS lithologies. In some cases, these contacts – typically poorly exposed – have been interpreted as detachments (presumably strands of the STFS), whereas they have been interpreted as depositional in others (Gehrels et al., 2003; Grujic et al., 2002; Robinson et al., 2006; Stöcklin, 1980). In Bhutan, both depositional and tectonic relationships have been reported for these outliers (e.g. Long and McQuarrie, 2010).

The South Tibetan fault system

The South Tibetan Fault system was first recognized in central Nepal (Caby et al., 1983) and later described in southern Tibet (Burchfiel et al., 1992; Burg and Chen, 1984) and northwest India (Herren, 1987; Searle, 1986; Valdiya, 1989). Although it comprises a variety of fault types

including steeply dipping transfer faults (Wu et al., 1998) and low-angle, oblique faults with a significant component of strike slip motion (Pêcher, 1991), most descriptions focus on the basal structure of the system, a low-angle, north-dipping fault and associated ductile shear zone commonly referred to as the South Tibetan detachment.

The presence of the STFS within a zone of continental collision has led to considerable debate regarding its initiation and role in the construction of the orogen (e.g. Hodges, 2000; Law et al., 2006 and references therein). Two principal models have been put forward to explain its existence. In the first, the STFS forms a collection of passive roof faults over an evolving contractional orogenic wedge (e.g. Robinson et al., 2006; Yin, 2006; Yin et al., 1994). In this case, the STFS has only a minor role in extrusion with minimal displacement across the structure and little excision of material in the footwall. In the second, the MCTS and STFS are kinematically linked structures that collectively sustained Miocene southward extrusion of the metamorphic core of the Himalaya (Beaumont et al., 2001; Godin et al., 2006 and references therein; Grujic et al., 2002; Hodges et al., 2001; Nelson et al., 1996). This concept, often referred to as the 'channel flow' model, implies that the STFS would have accommodated many kilometers of displacement and is responsible for excision of several kilometers of structural section within the GHS (Searle et al., 2006).

However, because of the geographic coincidence of many of the basal detachments with the Himalayan range crest and the relatively subdued relief north of the crest, most of these structures cannot be traced far down dip, and their net displacements are derived from indirect geothermobarometric measurements (15–200 km: Cottle et al., 2011; Cottle et al., 2007; Dèzes et al., 1999; Searle et al., 2003; Searle et al., 2002; Walker et al., 1999) and studies of fault-related telescoped isograds (25–170 km: Herren, 1987; Law et al., 2011). Exceptions occur in the Mount

Everest region of Nepal and the Mount Jomolhari region of NW Bhutan, where components of the STFS can be traced parallel to their slip vectors, with no match between correlative footwall and hanging wall units for ≥ 34 km in Nepal (Carosi et al., 1998; Hodges et al., 1992) and ≥ 65 km in Bhutan (Cooper et al., in press), implying minimum displacements comparable to ca. 75–140 km minimum estimates for broadly contemporaneous S-directed slip on the Main Central Thrust system (MCTS) in the eastern Himalaya (Yin, 2006; Yin et al., 2010).

The STFS footwall comprises high-grade (upper amphibolite facies) paragneisses and orthogneisses of the GHS with abundant leucogranite sills, dikes, and plutons. Near the top of the footwall, these rocks are strongly deformed and most exposures contain well-developed S-C mylonites (Lister and Snoke, 1984) indicative of hanging wall down-to-the north (normal-sense) shearing with varying degrees of oblique slip. In most mapped transects, the basal detachment carries ummetamorphosed lower Paleozoic sedimentary rocks of the TSS in its immediate hanging wall (e.g. Herren, 1987 (India); Hodges et al., 1993 (southern Tibet)). In two areas – the Annapurna Range of central Nepal (e.g., Brown and Nazarchuk (1993)) and the Everest region of eastern Nepal (e.g., Searle, 1999) – hanging wall TSS units also experienced greenschist to lower or middle amphibolite facies metamorphism, but the STFS still marks a significant discontinuity in metamorphic pressures and temperatures.

Studies of the STFS in Tibet (Burchfiel et al., 1992; Hodges et al., 1994) and Nepal (Hodges et al., 1996; Searle and Godin, 2003; Searle, 1999) show that wherever the basal detachment carries metamorphosed TSS rocks in its hanging wall, there is at least one major detachment of the STFS at a structurally higher level. These structures typically place stratigraphically younger TSS lithologies on older lithologies, or lower grade (or unmetamorphosed) rocks on higher grade rocks. The character of deformation along and above the STFS detachments depends on the

hanging wall lithology. Observations of the STFS in various localities in Nepal suggest that, when the basal detachment carries lower amphibolite or greenschist facies rocks in its hanging wall, there is typically a relatively wide shear zone above and below the detachment but often also a relatively sharp brittle-ductile shear zone at the contact itself (e.g. Deorali detachment: Hodges et al., 1996; Lhotse detachment: Searle, 1999; Annapurna detachment: Vannay and Hodges, 1996). Both ductile and brittle fabrics are transposed into parallelism with the detachment, indicating syn-detachment development. When the hanging wall is unmetamorphosed or weakly metamorphosed, there is a well-developed, relatively wide shear zone beneath the detachment and a usually pronounced (but sometimes thin) breccia zone at the contact. The breccia zone is oriented subparallel to the shear fabric in the footwall but the hanging wall-footwall contact is marked by an obvious cut-off of hanging wall strata, sometimes at a very high angle. Leucogranites cut the basal STFS detachment in several well-studied areas (e.g. Hodges et al., 1996), but examples of them cutting the upper detachment (e.g. Guillot et al., 1994; Hodges et al., 1998) are extremely rare.

The South Tibetan fault system in Bhutan and adjacent areas of Tibet

In the first regional study of the STFS, Burchfiel et al. (1992) mapped two transects across the GHS–TSS boundary just north of Bhutan at Wagye La and Lhozag-La Kang (Figure 1). In the Wagye La area, the contact is not exposed, but the topography and outcrop pattern indicate that it must dip shallowly northward, subparallel to well-developed S-C mylonitic planar fabrics in the footwall. The contact was interpreted by Burchfiel et al. (1992) as a segment of the basal detachment of the STFS, with classic GHS footwall units including amphibolite facies orthogneisses and psammitic and pelitic schists, all intruded by leucogranite sills and dikes. The

hanging wall units (low-grade Ordovician marbles and phyllites) are themselves cut by a well-exposed upper detachment that carries unmetamorphosed Carboniferous-Permian limestones in its hanging wall.

At Lhozag La Kang, the principal STFS detachment has been deformed into ca. 10 km-wavelength, upright folds and subsequently cut by steeply N-dipping, E-striking normal faults with relatively minor displacement (Burchfiel et al., 1992; Edwards et al., 1999). This detachment cuts and thus postdates the ca. 12.5 Ma Khula Kangri leucogranite pluton (Edwards and Harrison, 1997) (Figure 1). At Gonto La (Edwards et al., 1996) (Figure 1), the detachment also cuts an older, structurally lower STFS detachment that is intruded by the Khula Kangri pluton.

In the central latitudes of Bhutan, Gansser (1983) mapped synformal erosional remnants of TSS lithologies above GHS units far south of the main outcrop trace of the STFS along the Bhutan-Tibet border (Figure 1). The structurally and stratigraphically highest units in the erosional remnants are Precambrian-Devonian(?), locally fossiliferous, low-grade calc-schists, calcarenites, and limestones of the Pele La Group and the Tang Chu Group (Hughes et al., 2011; Long and McQuarrie, 2010; Tangri and Pande, 1995), similar to basal TSS lithologies widespread in the Himalaya and southern Tibet (Dèzes et al., 1999; Gansser, 1964; Hodges et al., 1996; Le Fort, 1975; Searle and Godin, 2003; Searle et al., 2003). The rocks mapped as GHS throughout Bhutan comprise Proterozoic-Ordovician(?) granitic and migmatitic orthogneiss, migmatitic metasedimentary rocks, schist, paragneiss, quartzite, and discrete marble bands, pervasively intruded by Miocene leucogranites (Bhargava, 1995; Davidson et al., 1997; Gansser, 1983; Grujic et al., 2002; Hollister and Grujic, 2006; Long and McQuarrie, 2010; Long et al., 2011c; Swapp and Hollister, 1991). There is little controversy regarding correlations of these

224 rocks with GHS units elsewhere in the Himalaya. Of less certain affinity is a unit interposed
225 between classically GHS and TSS units referred to as the Chekha Formation (Gansser, 1983;
226 Jangpangi, 1974; Nautiyal et al., 1964; Tangri and Pande, 1995).

227 The Chekha Formation in Bhutan comprises non-fossiliferous greenschist to amphibolite
228 facies metapelite, paragneiss, augen gneiss, quartzite and calc-silicate intruded by leucogranite
229 sills and dikes (Cooper et al., in press; Gansser, 1983; Grujic et al., 2002; Kellett et al., 2009;
230 Long and McQuarrie, 2010; McQuarrie et al., 2008). Kellett et al. (2009); Kellett et al. (2010);
231 and Kellett and Grujic (2012) correlated the Chekha regionally with TSS units in other parts of
232 the Himalaya, notably the Everest Series and North Col Formation of eastern Nepal (Searle et al.,
233 2003), the Annapurna Yellow Formation of central Nepal (Gleeson and Godin, 2006), and the
234 Haimanta Group of NW India (Chambers et al., 2009). If this is the case, then age constraints for
235 these other units suggest a probable Cambrian age for the Chekha (Burchfiel et al., 1992; Carosi
236 et al., 1999; Colchen et al., 1986; Frank et al., 1973; Lombardo et al., 1993; Mu et al., 1973;
237 Myrow et al., 2009; Wang and Zhen, 1975). Other workers have used the position of the Chekha
238 at the base of the TSS and its lack of fossils to infer a Precambrian age (Gansser, 1983; Tangri
239 and Pande, 1995) for the unit. Detrital zircon U-Pb age spectra from some Chekha samples are
240 similar to those obtained for TSS samples, whereas others are more like those obtained for GHS
241 samples collected in Bhutan (Gehrels et al., 2011; Hughes et al., 2011; Long and McQuarrie,
242 2010; McQuarrie et al., 2008). As Hughes et al. (2011) note, additional stratigraphic constraints
243 on the depositional age of the Chekha Formation are needed.

244 The contacts between the Chekha Formation and units above and below have been variably
245 interpreted. Gansser (1983) described the GHS–Chekha contact as conformable and noted that
246 both the uppermost GHS pelitic units and the lowermost Chekha Formation schists contain

247 distinct biotite porphyroblasts (cross-biotites) lying perpendicular to foliation but parallel to
248 lineation. Grujic et al. (2002), on the other hand, found evidence for a diffuse top-to-the-north
249 shear zone (width unconstrained) at the base of the Chekha Formation across Bhutan, and re-
250 interpreted the Dang Chu (or Tang Chu), Ura, Zhemgang (or Black Mountain), and Sakteng (or
251 Radi) exposures as klippen soled by the STFS basal detachment. Their main lines of evidence
252 were: (1) Top-to-the-north shear sense indicators at the top of the GHS and the base of the
253 Chekha Formation; (2) The presence of migmatite and sillimanite in the GHS that are absent
254 from the Chekha Formation above; and (3) An upsection decrease in metamorphic grade within
255 the Chekha Formation. However, despite these first-order observations across Bhutan, no
256 discrete (meter-scale) brittle-ductile shear zone at the contact, upward increase in strain towards
257 the contact, or definitive structural discordance between footwall and hanging wall units has yet
258 been described at this structural level (e.g. Carosi et al., 2006; Grujic et al., 2002; Kellett et al.,
259 2009), contrary to observations of classic STFS detachments in other parts of the Himalaya (e.g.
260 Burchfiel et al., 1992; Hodges et al., 1992; Hodges et al., 1996; Pognante and Benna, 1993;
261 Searle et al., 1997; Searle, 1999; Vannay and Hodges, 1996).

262 The ambiguity in the GHS–Chekha contact is exemplified by the contrasting mapping of two
263 different groups working in Bhutan, which shows little agreement on either the position or the
264 nature of the contact. Long and McQuarrie (2010), for example, largely followed the original
265 mapping by Gansser (1983), and agreed with Grujic et al. (2002) that the base of the Chekha
266 Formation in the Dang Chu, Ura, and Sakteng klippen was a top-to-the-north shear zone of the
267 STFS. However, in contrast to Grujic et al. (2002), they suggested that interfingering of GHS
268 and Chekha units at the base of the Zhemgang klippe in southern Bhutan indicated a depositional
269 contact there (Figures 2a and 5). Grujic et al. (2011), on the other hand, map the Chekha to a far

greater extent throughout central Bhutan, combining the Dang Chu and Zhemgang klippe into a single entity, and extending the Ura klippe northward, where it is cut by the KT (Figure 2b). A direct comparison between the maps of the two groups (Figure 2) suggests that the large areal extent of the Chekha mapped by Grujic et al. (2012) corresponds closely to the extent of the GHS metasedimentary unit mapped by Long and McQuarrie (Figure 5). This again reinforces the ambiguity between the two lithologic units and suggests that new data is needed to understand the structural relationship between them.

The difference in mapping of the STFS in central Bhutan has implications for the magnitude of displacement on the STFS. The interpretation by Long and McQuarrie (2010) that the base of the Zhemgang klippe is a conformable contact between GHS and TSS units but the base of the Ura klippe is a strand of the STFS led them to argue that the breakaway zone for the STFS must lie in between the two (Figures 2a and 3a). If this is the case then it limits slip on the STFS to a maximum of only 20 km, and reduces the significance of extensional faulting as a major orogen-building process. In contrast, mapping of STFS detachments (including at the base of the Zhemgang klippe) by Grujic et al. (2012) as far as 100 km south of the main STFS trace along the Himalayan range crest, with no observed breakaway zone, means that STFS hanging-wall-on-footwall relationships can be traced in the direction of slip for ca. 100 km, implying large displacements on this system.

Thermobarometric studies across the GHS–Chekha contact in Bhutan are limited. Studies by Davidson et al. (1997) and Daniel et al. (2003) found the GHS to have reached peak metamorphic temperatures of 600–750°C and pressures of 8–10 kbar. In a detailed thermobarometric study across the Ura klippe based on silicate mineral compositions, Kellett et al. (2010) infer a change in temperature across the GHS–Chekha contact, but see no discernable

change in pressure. On closer inspection, their data show a similarly large spread in pressure-temperature (*P-T*) conditions for both the Chekha Formation (576–730°C and 6.9–8.7 kbar) and the GHS (560–789°C and 8.0–9.1 kbar), indicating no metamorphic discontinuity across this contact. Their results are similar in the Jomolhari region of NW Bhutan (referred to by the authors as the Lingshi klippe), where one sample from the base of the Chekha Formation gives a *P-T* of 721°C and 8.7 kbar, while 6 samples from the GHS give a spread of 622–787°C and 6.2–10.9 kbar. Thermobarometric data from a recent study across the GHS-Chekha contact at the base of the Zhemgang klippe by Corrie et al. (2012) supports the interpretation of Long and McQuarrie (2010) that it is a conformable contact, noting a gradual change in peak temperature and pressure across the contact from ca. 540–620°C and 9 kbar in the GHS approximately 2 km from the contact to 550°C and 7.5 kbar throughout the Chekha Formation. In the only other RSCM study in Bhutan to date, Kellett and Grujic (2012) obtained peak RSCM temperatures from Chekha and TSS rocks of the Linghsi klippe that show little variation, with a consistently low peak temperature of ca. 300°C. By combining these RSCM data with the *P-T* data of Kellett et al. (2010), Kellett and Grujic (2012)inferred a gradual change in temperature across the GHS–Chekha contact, which they ascribed to a diffuse shear zone at this structural level. However, the substantial drop in temperature to ca. 300°C is approximately 600 m above this contact, suggesting a more significant offset at a structurally higher position.

The nature of the contact between the Chekha Formation and the overlying indisputable TSS (Pele La Group and Tang Chu Group) is also unclear. Exposed in the Mount Jomolhari region in NW Bhutan and in the Dang Chu klippe (We refer to it as such because it is cut by the Dang Chu river. It is usually referred to as the Tang Chu klippe after Gansser (1983), but this is a potential source of confusion because the Tang Chu actually river lies to the east near the Ura klippe) in

316 central Bhutan, Gansser (1983) and Carosi et al. (2006) mapped it as a conformable contact, but
317 Edwards et al. (1996), Hollister and Grujic (2006), and Chambers et al. (2011) interpreted it as
318 an STFS detachment. In NW Bhutan (Figure 1), Cooper et al. (in press) mapped recumbently
319 folded fossiliferous marbles of the TSS above amphibolite facies metapelites, calc-silicates, and
320 leucogranites of the Chekha Formation. The abrupt change in structural style across the contact
321 between these two units together with the stark change in lithology and metamorphic grade led
322 the authors to interpret this contact as a detachment of the STFS.

323 In the Dang Chu klippe, Gansser (1983) mapped two isolated exposures of the TSS lying
324 above the Chekha Formation. In the more accessible northern exposure, the transition from
325 Chekha Formation to TSS units of the Pele La Group and Tang Chu Group is marked by a
326 dramatic change in structural style from foliated metapelites and quartzites to recumbently folded
327 calc-silicates and marbles (Figure 4a-c). Just to the east of the southern TSS exposure mapped by
328 Gansser (1983), Hughes et al. (2011) identified Cambrian brachiopod and trilobite fossils in
329 siliciclastic and carbonate units of the Pele La Group. Although this location has been mapped by
330 other researchers as part of the Chekha Formation (Grujic et al., 2002; Grujic et al., 2011; Kellett
331 et al., 2009; Kellett et al., 2010; Long and McQuarrie, 2010; Long et al., 2011c), we join Hughes
332 et al. (2011) as interpreting these fossiliferous outcrops as part of the TSS and have extended the
333 southern exposure of this unit in the Dang Chu klippe eastward to include this locality (Figure 1).

334 Above the Chekha Formation in the center of the Zhemgang klippe (Figure 4e), Long and
335 McQuarrie (2010) mapped the Maneting Formation, a biotite-garnet bearing phyllitic unit
336 (Figure 4f) of the Pele La group (Tangri and Pande, 1995). Based on an observed upsection
337 transition from Chekha quartzite to Maneting phyllite and interfingering of the two lithologies,
338 they interpreted the contact between the Chekha and Maneting Formations to be conformable

(Figures 2a and 5). Thermobarometric data from Corrie et al. (2012) agree with this interpretation, suggesting a steady decrease in peak *P-T* conditions across the Chekha-Maneting contact, with no evidence for a structural break.

Because structural studies alone do not seem sufficient to determine the nature of the GHS–Chekha and Chekha–TSS contacts in the central latitudes of Bhutan, we applied thermometric techniques to evaluate the evidence for a metamorphic discontinuity across them. Although conventional pelitic thermobarometers are easily applied to many GHS rocks, Chekha Formation and TSS rocks typically contain less suitable high-variance mineral assemblages. As a consequence, we focused our studies on the establishment of peak metamorphic temperatures through the more widely-applicable Raman spectroscopy on carbonaceous material (RSCM) method. This relatively new technique (Aoya et al., 2010; Beyssac et al., 2002a; Beyssac et al., 2002b; Rahl et al., 2005) has become very popular in recent years and has been applied to rocks from several sectors of the Himalayan orogen (Beyssac et al., 2004; Bollinger et al., 2004; Célérier et al., 2009; Cottle et al., 2011; Kellett and Grujic, 2012). The popularity of the RSCM thermometer stems from its applicability to rocks of many bulk compositions, the fact that it is apparently independent of metamorphic pressure (unlike most of the commonly used metamorphic thermometers for amphibolite facies metamorphic rocks), and its resistance to retrograde resetting during protracted or polyphase metamorphism.

RSCM THERMOMETRY

Carbonaceous material (CM) is a common constituent of metasedimentary rocks, deriving from the solid-state metamorphic transformation of original organic material (Buseck and Huang, 1985). During diagenesis and metamorphism this CM experiences progressive structural

organization until it transforms into graphite. The degree of organization is independent of pressure but strongly dependent on temperature such that the CM can be used as an indicator of metamorphic grade (Beyssac et al., 2002a; Beyssac et al., 2002b; Rietmeijer and Mackinnon, 1985; Wopenka and Pasteris, 1993). Beyssac et al. (2002a) demonstrated that peak metamorphic temperature (T) can be estimated in the range 330–650°C with a nominal uncertainty of ± 50°C (1σ) by measuring the peak area ratio (R2) of characteristic CM bands (D1, D2, G: Figure 6) in the Raman spectrum and inputting this parameter into the equation: $T(°C) = -445\ R2 + 641$.

Rahl et al. (2005) devised an alternative calibration of the RSCM thermometer that extends its range to 100–700°C. In this calibration, peak metamorphic temperature is calculated from both the peak area ratio (R2) of Beyssac et al. (2002a) and the peak height ratio (R1) of CM bands D1 and G. Temperature is calculated using the equation: $T(°C) = 737.3 + 320.9\ R1 - 1067\ R2 - 80.638\ R1^2$. However, both of these calibrations were made using a micro-Raman system with a 514 nm wavelength laser. At Arizona State University we use a 532 nm laser, which results in a slightly, but systematically larger R2 ratio than that of a 514.5 nm laser (Aoya et al., 2010). To account for this difference, Aoya et al. (2010) derived a new 532 nm laser calibration in which the temperature is calculated using the equation: $T(°C) = 221.0\ R2^2 - 637.1\ R2 + 672.3$, where the R2 ratio derives from the original Beyssac et al. (2002a) calibration. The Aoya et al. (2010) calibration is valid for samples in the range 340–655°C and we use this for all of our RSCM calculations.

Sampling and analysis

We collected 17 samples for RSCM analysis across the Dang Chu klippe, the Ura klippe, and the Zhemgang klippe, encompassing rocks of the GHS, Chekha Formation, and TSS (Figure 2).

385 Lithologies include paragneiss, pelitic schist, calc-silicate, slate, phyllite, and marble (Table 1).
386 Laser Raman analyses of CM were made on microprobe-quality polished petrographic thin
387 sections. In order to avoid variations in mineral orientation and anisotropy on the Raman spectra
388 (Beyssac et al., 2002a; Katagiri et al., 1988), thin sections were cut normal to foliation and
389 parallel to stretching lineation (when present).

390 Measurements were made using a custom-built Raman spectrometer in the LeRoy Eyring
391 Center for Solid State Science at Arizona State University. The sample was excited using a
392 Coherent *Compass* laser, with power controlled using neutral density filters. The laser was
393 focused onto the sample using a ×50 Mitutoyo objective, and the signal was discriminated from
394 the laser excitation with a Kaiser laser band pass filter followed by a Semrock edge filter. The
395 system has a spectral resolution of 3.5 cm^{-1} using a 1200 g/mm grating and a spatial resolution of
396 <1 μm with the ×50 objective lens. In order to avoid any mechanical disruption of the CM from
397 the thin section making and polishing process (Beyssac et al., 2003), the laser was typically
398 focused on CM situated beneath the surface of a transparent grain of quartz or calcite (Data
399 Repository Item A). The data were collected using an Acton 300i spectrograph and a back
400 thinned Princeton Instruments liquid nitrogen cooled CCD detector. Grains of CM were analyzed
401 with a 3 mW beam for 120 seconds over a spectral window of 1100 to 2000 cm^{-1}. Depending on
402 the abundance of CM, between 15 and 25 grains were analyzed in each sample in order to
403 evaluate the degree of in-sample heterogeneity. Peak positions, band areas and band widths of
404 the resulting Raman spectra were determined with the computer program PeakFit 4.12 (Systat
405 Software Inc.).

406

407 **Results**

All temperatures were calculated using the 532 nm laser calibration of Aoya et al. (2010) and are given in Table 1. For comparison, we also calculated temperatures with the Beyssac et al. (2002b) and Rahl et al. (2005) 514 nm laser calibrations, which gave results in close agreement (Data Repository Item B). Examples of Raman spectra for each sample are shown in Figure 6 together with R2 values and calculated temperatures. Photographs of representative CM grains from selected samples can be found in Data Repository Item A.

In Table 1, the variation in R2 within each sample is indicated by the standard deviation (1σ). CM heterogeneity can result from differences in the original organic material, variations in the structure of the CM, the influence of the mineral matrix (e.g. shielding of CM within porphyroclasts), or the composition of metamorphic fluids (Beyssac et al., 2002a; Beyssac et al., 2002b; Large et al., 1994). The average variation in R2 for the 17 samples is 0.095, which corresponds to a temperature difference of ± 50°C. Sample FB132 has the highest variation in R2 at ± 0.122, which corresponds to a temperature difference of ± 75°C.

Temperatures calculated using the calibration of Aoya et al. (2010) are reported as standard means of multiple measurements from each sample. The internal uncertainty on our analytical procedures is reflected by the variation in temperature within each sample, and is reported as 1 standard deviation on the mean. However, for each individual value of R2, there is also an associated external uncertainty on the calculated temperature of ± 50°C stemming from the original calibration of CM organization against independent *P-T* data (Beyssac et al., 2002a). Therefore, in order to report a complete and more accurate uncertainty, we added our internal and external uncertainties in quadrature before dividing by the square root of the number of analyses per sample. Final temperatures are thus reported at 2 standard errors of the mean (Table 1 and Data Repository Item B).

Thirteen samples from Chekha and GHS units give very consistent temperatures, with an error-weighted mean average of 560 ± 2°C (2SE) (Figures 2, 7, and 9). The only change in peak temperature is seen in four samples across the Dang Chu klippe. Two foliated calc-silicates on the NW edge of the klippe, samples FB64, and FB85, give slightly lower peak temperatures of 508 ± 33°C and 489 ± 26°C, respectively. The lowest temperatures are seen in samples FB28, a folded marble collected at Pele La within the northern TSS exposure (Figure 4b), and FB77, a black slate located on the W side of the klippe in the Chekha Formation. These give temperatures 130–140°C lower than the majority of the samples at 430 ±30°C and 420 ± 21°C, respectively.

Comparison with GARB-GMBP thermometry

In order to verify the temperatures calculated with the RSCM method, we conducted independent *P-T* calculations on three of the 17 samples. Samples FB07, FB125, and FB132 have a mineral assemblage of garnet + biotite + muscovite + plagioclase, permitting the application of the well-established GARB (garnet-biotite) exchange thermometer (Ferry and Spear, 1978) and GMBP (garnet-muscovite-biotite-plagioclase) net-transfer barometer (Ghent and Stout, 1981). In order to minimize sources of uncertainty in the thermobarometric calculations, we followed the approach of Cooper et al. (2010) by characterizing textural and geochemical relationships in detail and conducting multiple independent calculations on each sample. For more details, see Data Repository Item C.

Mineral composition data were obtained with a JEOL JXA-8200 electron microprobe at the University of California, Los Angeles and a Cameca SX50 electron microprobe at the University of Massachusetts. Thermobarometric calculations were made using THERMOCALC v. 3.33 software (Powell and Holland, 1988), and the latest version of the Holland and Powell data set

(Holland and Powell, 1998). Activity-composition relationships were calculated using the AX program (Tim Holland: http://www.esc.cam.ac.uk/research/research-groups/holland/ax). Individual *P-T* calculations and representative mineral analyses can be found in Data Repository Items D and E.

RSCM temperatures and GARB-GMBP temperatures and pressures for each sample are given in Table 2 for comparison. The results show that there is good agreement between the three independent temperature measurements within the limits of the uncertainties on both methods and the pressure estimates on the three samples are also consistent, with an error-weighted mean pressure of 5.2 ± 0.5 kbar (2SE).

IMPLICATIONS FOR THE STFS IN CENTRAL BHUTAN

The lack of either a distinct discontinuity or a progressive change in temperature across the base of both the Dang Chu and Ura klippen, and similar temperatures in the center of the Zhemgang klippe raises questions about the interpretation of the GHS–Chekha contact being a strand of the STFS. In contrast, the lower peak temperatures reached by four samples in the Dang Chu klippe point to a likely detachment between the Chekha Formation and overlying TSS sediments, an interpretation supported by the change in structural style observed in rocks above and below the contact (Figure 4).

The interpretation that there is no structural discontinuity between the GHS and the Chekha Formation is consistent with the conclusion reached by Long and McQuarrie (2010) that the Chekha Formation of the Zhemgang klippe (which they interpret as part of the TSS) is in depositional contact with the GHS (Figures 1 and 2a). However, we disagree with Long and McQuarrie (2010) regarding the broader tectonic significance of that observation. We suggest

477 that the Chekha Formation and overlying Maneting Formation are in the STFS footwall, and that
478 the absence of evidence for fault slip at the GHS–Chekha contact in the Zhemgang klippe is not
479 surprising as a consequence. On the other hand, the TSS units that give low peak temperatures of
480 420–430°C coincide with recumbently folded marbles that exhibit a wholly different structural
481 style to both the Chekha and GHS units below (Figure 4). Although we have not found
482 fossiliferous marbles in the northern TSS Dang Chu exposure, the fossils found to the south by
483 Hughes et al. (2011) are from the TSS. If similar fossiliferous beds are present in the northern
484 part of the klippe, they must lie at structurally higher elevations that have so far proved
485 inaccessible. The strongly foliated, high-strain calc-silicate samples FB64 and FB85, which give
486 intermediate peak temperatures of ca. 490–510°C, are interpreted as basal units of the TSS that
487 have been heated and transposed by shearing along the STFS detachment. They therefore
488 roughly define the position of the STFS shear zone.

489 Figure 8a shows our interpretation for the distribution of RSCM temperatures in central
490 Bhutan. The Chekha Formation and GHS are combined as one sequence in the figure, although
491 our data and observations do not speak to whether or not the two are separated by a major
492 unconformity. We propose a different map pattern for the TSS in the Dang Chu area that
493 includes the four lower-temperature samples FB28, FB64, FB77 and FB85, and we interpret the
494 contact between the TSS and structurally lower units to be the sole STFS detachment. The high-
495 strain calc-silicate samples FB64 and FB85 are mapped at the base of the TSS, and we suggest
496 that their slightly higher peak temperatures result from shear heating along the STFS shear zone.
497 This interpretation is consistent with all outcrops we have seen in the area, but the quality of
498 outcrop is so poor that detailed field confirmation of this map pattern is difficult.

499 If our interpretation is correct, it suggests that to truly understand the kinematics and

displacement history of the STFS, we need to focus on this upper contact in the Dang Chu area, not on the previously mapped GHS–Chekha contacts. Our interpretation is inconsistent with the contention by Long and McQuarrie (2010) that the stratigraphic contact between TSS and GHS units in the Zhemgang klippe can be used to place a limit of ca. 20 km on STFS displacement and thus the magnitude of putative channel flow. The presence of TSS units ca. 80 km south of the Himalayan range crest suggests that displacement on the STFS may in fact be even greater than previously thought (Figure 8b).

An alternative interpretation of the geology that fits with our data is that of Grujic et al. (2011), who map the Chekha Formation more extensively across Bhutan (Figure 2b). According to their mapping, the majority of RSCM samples that give a consistent temperature of ca. 560°C are situated within the Chekha Formation. The exceptions are samples FB125 and FB132, which lie within the GHS on the edge of the Dang Chu klippe and samples BT1134, BT1136, and BT1138, which lie within the Maneting Formation in the Zhemgang klippe. However, we do not favor their interpretation as we see no evidence for a discrete shear zone at any of the GHS–Chekha contacts mapped and we have found paragneisses reasonably attributed to the GHS within areas mapped as Chekha Formation by Grujic et al. (2011) in both the Dang Chu and Ura klippen. Grujic et al. (2011) also map the TSS very differently in the Dang Chu klippe, with no clear explanation as to why. The folded marbles at Baylangdra (Figure 4a) are mapped as part of the TSS but at Pele La (Figure 4b) they are mapped as Chekha. This is inconsistent with both our temperature and structural data.

CONCLUSIONS

RSCM thermometry data from 17 samples combined with structural observations across three purported STFS klippen in central Bhutan suggest that current maps of this structure require revision. We find no change in peak metamorphic temperature across the contact between Chekha Formation rocks and underlying indisputable GHS units. Instead, we see a 130–140°C drop in temperature across an upper contact between the Chekha Formation and Precambrian-Devonian(?) TSS sediments of the Pele La and Tang Chu Groups. We therefore see no reason to infer that the Chekha Formation and the GHS are separated by the basal strand of the STFS. We regard the upper contact between the Chekha Formation and indisputable TSS units as the sole STFS detachment, and suggest that future studies of the kinematics and displacement on this system should be focused on this upper contact. The lack of matching hanging wall and footwall lithologic units or metamorphic grade in the direction of STFS motion suggests that displacement on the STFS may be as much as ca. 80 km, not less than ca. 20 km as suggested by Long and McQuarrie (2010). In light of the new data presented here, there is no clear evidence for a breakaway zone for the STFS in southern Bhutan.

ACKNOWLEDGEMENTS

This work was supported by US National Science Foundation grant EAR-0838112 to K.V.H. We thank Emmanuel Soignard of the LeRoy Eyring Center for Solid State Science at ASU for his help with the Raman spectrometer, and Frank Kyte at UCLA and Michael Jercinovic at the University of Massachusetts for their assistance with the electron microprobe analyses. Field work would not have been possible without assistance from Kelin Whipple and Arjun Heimsath and the support of our friends and colleagues in Bhutan: Peldon Tshering (National Environment Commission), Ugyen Wanda (Department of Geology and Mines), Karma Choden and Ugyen

Rinzen (Yangphel Adventure Travel). Detailed and constructive reviews by editor Eric Kirby and two anonymous reviewers are gratefully acknowledged.

REFERENCES CITED

Acharyya, S. K., and Sastry, M., 1979, Stratigraphy of the eastern Himalaya: Geological Survey of India Miscellaneous Publications, v. 41, p. 49-67.

Aoya, M., Kouketsu, Y., Endo, S., Shimizu, H., Mizukami, T., Nakamura, D., and Wallis, S., 2010, Extending the applicability of the Raman carbonaceous-material geothermometer using data from contact metamorphic rocks: Journal of Metamorphic Geology, v. 28, no. 9, p. 895-914, doi: 10.1111/j.1525-1314.2010.00896.x.

Beaumont, C., Jamieson, R. A., Nguyen, M. H., and Lee, B., 2001, Himalayan tectonics explained by extrusion of a low-viscosity crustal channel coupled to focused surface denudation: Nature, v. 414, p. 738-742.

Beyssac, O., Bollinger, L., Avouac, J.-P., and Goffé, B., 2004, Thermal metamorphism in the lesser Himalaya of Nepal determined from Raman spectroscopy of carbonaceous material: Earth and Planetary Science Letters, v. 225, p. 233-241.

Beyssac, O., Goffe, B., Chopin, C., and Rouzaud, J., 2002a, Raman spectra of carbonaceous material in metasediments: a new geothermometer: Journal of Metamorphic Geology, v. 20, no. 9, p. 859-871.

Beyssac, O., Goffé, B., Petitet, J.-P., Froigneux, E., Moreau, M., and Rouzaud, J.-N., 2003, On the characterization of disordered and heterogeneous carbonaceous materials by Raman spectroscopy: Spectrochimica Acta Part A, v. 59, p. 2267-2276.

567 Beyssac, O., Rouzaud, J.-N., Goffé, B., Brunet, F., and Chopin, C., 2002b, Graphitization in a
568 high-pressure, low-temperature metamorphic gradient: a Raman microspectroscopy and
569 HRTEM study: Contributions to Mineralogy and Petrology, v. 143, p. 19-31.
570 Bhargava, O. N., 1995, The Bhutan Himalaya: A Geological Account, Geological Society of
571 India Special Publication, Calcutta, 245 p.
572 Bollinger, L., Avouac, J. P., Beyssac, O., Catlos, E. J., Harrison, T. M., Grove, M., Goffé, B.,
573 and Sapkota, S., 2004, Thermal structure and exhumation history of the Lesser Himalaya
574 in central Nepal: Tectonics, v. 23, no. 5, p. 1-19, doi: 10.1029/2003TC001564.
575 Brasier, M. D., and Singh, P., 1987, Microfossils and Precambrian-Cambrian boundary
576 stratigraphy at Maldeota, Lesser Himalaya: Geological Magazine, v. 124, p. 323-345.
577 Brookfield, M. E., 1993, The Himalayan passive margin from Precambrian to Cretaceous times:
578 Sedimentary Geology, v. 84, p. 1-35.
579 Brown, R. L., and Nazarchuk, J. H., 1993, Annapurna detachment fault in the Greater Himalaya
580 of central Nepal, *in* Treloar, P. J., and Searle, M. P., eds., Himalayan Tectonics, Volume
581 74: London, Geological Society Special Publication, p. 461-473, doi:
582 10.1144/GSL.SP.1993.074.01.31.
583 Burbank, D. W., Beck, R. A., and Mulder, T., 1997, The Himalayan foreland basin, *in* Yin, A.,
584 and Harrison, M., eds., The tectonic evolution of Asia: Cambridge, Cambridge University
585 Press, p. 149-188.
586 Burchfiel, B. C., Zhiliang, C., Hodges, K. V., Yuping, L., Royden, L. H., Changrong, D., and
587 Jiene, X., 1992, The South Tibetan Detachment System, Himalayan Orogen: Extension
588 Contemporaneous With and Parallel to Shortening in a Collisional Mountain Belt, 41 p.

589 Burg, J. P., and Chen, G. M., 1984, Tectonics and structural zonation of southern Tibet, China:
590 Nature, v. 311, p. 219-223.
591 Buseck, P. R., and Huang, B.-J., 1985, Conversion of carbonaceous material to graphite during
592 metamorphism: Geochimica et Cosmochimica Acta, v. 49, p. 2003-2016.
593 Caby, R., Pêcher, A., and Le Fort, P., 1983, Le grande chevauchement central himalayen:
594 Nouvelles données sur le métamorphisme inverse à la base de la Dalle du Tibet: Revue
595 de Géographie Physiqueau et Géologie Dynamique, v. 24, p. 89-100.
596 Carosi, R., Lombardo, B., Musumeci, G., and Pertusati, P. C., 1999, Geology of the Higher
597 Himalayan Crystallines in the Khumbu Himal (Eastern Nepal): Journal of Asian Earth
598 Sciences, v. 17, p. 785-803.
599 Carosi, R., Molli, B. L., Musumeci, G., and Pertusati, P. C., 1998, The south Tibetan detachment
600 system in the Rongbuk valley, Everest region: Deformation features and geological
601 implications: Journal of Asian Earth Sciences, v. 16, p. 299-311.
602 Carosi, R., Montomoli, C., Rubatto, D., and Visona, D., 2006, Channel Flow, Ductile Extrusion
603 and Exhumation in Continental Collision Zones, *in* Law, R., Searle, M., and Godin, L.,
604 eds., Volume 268, Geological Society London Special Publication, p. 425-444.
605 Célérier, J., Harrison, T. M., Beyssac, O., Herman, F., Dunlap, W. J., and Webb, A. A. G., 2009,
606 The Kumaun and Garwhal Lesser Himalaya, India: Part 2. Thermal and deformation
607 histories: Geological Society of America Bulletin, v. 121, no. 9/10, p. 1281-1297, doi:
608 10.1130/B26343.1.
609 Chakungal, J., Dostal, J., Grujic, D., Duchêne, S., and Ghalley, K. S., 2010, Provenance of the
610 Greater Himalayan sequence: Evidence from mafic granulites and amphibolites in NW
611 Bhutan: Tectonophysics, v. 480, p. 198-212.

612 Chambers, J., Caddick, M., Argles, T., Horstwood, M., Sherlock, S., Harris, N., Parrish, R., and
613 Ahmad, T., 2009, Empirical constraints on extrusion mechanisms from the upper margin
614 of an exhumed high-grade orogenic core, Sutlej valley, NW India: Tectonophysics, v.
615 477, p. 77-92.
616 Chambers, J., Parrish, R., Argles, T., Harris, N., and Horstwood, M., 2011, A short duration
617 pulse of ductile normal shear on the outer South Tibetan detachment in Bhutan:
618 alternating channel flow and critical taper mechanics of the eastern Himalaya: Tectonics,
619 v. 30, doi: 10.1029/2010TC002784.
620 Colchen, M., LeFort, P., and Pêcher, A., 1986, Annapurna-Manaslu-Ganesh Himal., Paris,
621 Centre National de la Recherche Scientifique, 136 p.
622 Cooper, F. J., Adams, B. A., Edwards, C. S., and Hodges, K. V., in press, Large normal-sense
623 displacement on the South Tibetan fault system in the eastern Himalaya: Geology, doi:
624 10.1130/G33318.1.
625 Cooper, F. J., Platt, J. P., Anczkiewicz, R., and Whitehouse, M. J., 2010, Footwall dip of a core
626 complex detachment fault: thermobarometric constraints from the northern Snake Range
627 (Basin and Range, USA): Journal of Metamorphic Geology, doi: 10.1111/j.1525-
628 1314.2010.00907.x.
629 Corrie, S. L., Kohn, M. J., McQuarrie, N., and Long, S. P., 2012, Flattening the Bhutan
630 Himalaya: Earth and Planetary Science Letters, v. 349-350, p. 67-74, doi:
631 10.1016/j.epsl.2012.07.001.
632 Cottle, J., Waters, D., Riley, D., Beyssac, O., and Jessup, M. J., 2011, Metamorphic history of
633 the South Tibetan Detachment System, Mt. Everest region, revealed by RSCM

thermometry and phase equilibria modelling: Journal of Metamorphic Geology, v. 29, p. 561-582.

Cottle, J. M., Jessup, M. J., Newell, D. L., Searle, M. P., Law, R. D., and Horstwood, M. S. A., 2007, Structural insights into the early stages of exhumation along an orogen-scale detachment: The South Tibetan Detachment System, Dzakaa Chu section, Eastern Himalaya: Journal of structural geology, v. 29, p. 1781-1797.

Critelli, S., and Garzanti, E., 1994, Provenance of the lower Tertiary Murree redbeds (Hazara-Kashmir syntaxis, Pakistan) and initial rising of the Himalayas: Sedimentary Geology, v. 89, p. 265-284.

Daniel, C. G., Hollister, L. S., Parrish, R., and Grujic, D., 2003, Exhumation of the Main Central Thrust from Lower Crustal Depths, Eastern Bhutan Himalaya: Journal of Metamorphic Geology, v. 21, p. 317--334.

Davidson, C., Grujic, D. E., Hollister, L. S., and Schmid, M., 1997, Metamorphic reactions related to decompression and synkinematic intrusion of leucogranite, High Himalayan Crystallines, Bhutan: Journal of Metmorphic Geology, v. 15, p. 593-612.

de Sigoyer, J., Chavagnac, V., Blichert-Toft, J., Villa, I. M., Luais, B., Guillot, S., Cosca, M., and Mascle, G., 2000, Dating the Indian continental subduction and collisional thickening in the northwest Himalaya: multichronology of the Tso Morari eclogites: Geology, v. 28, p. 487-490.

DeCelles, P. G., Gehrels, G. E., and Quade, J., 1998, Eocene-early Miocene foreland basin development and the history of Himalayan thrusting, western and central Nepal: Tectonics, v. 17, p. 741-765.

656 Dèzes, P. J., Vannay, J.-C., Steck, A., Bussy, F., and Cosca, M., 1999, Synorogenic extension;
657 quantitative constraints on the age and displacement of the Zanskar shear zone (northwest
658 Himalaya): Geological Society of America Bulletin, v. 111, no. 3, p. 364-374.
659 Edwards, M., Kidd, W., Li, J., Yue, Y., and Clark, M., 1996, Multi-stage development of the
660 southern Tibetan detachment system near Khula Kangri. New data from Gonto La:
661 Tectonophysics, v. 260, p. 1-19.
662 Edwards, M., Pêcher, A., Kidd, W., Burchfiel, B., and Royden, L., 1999, Southern Tibet
663 Detachment System at Khula Kangri, Eastern Himalaya: A Large-Area, Shallow
664 Detachment Stretching into Bhutan?: The Journal of Geology, v. 107, p. 623-631.
665 Edwards, M. A., and Harrison, T. M., 1997, When did the roof collapse? Late Miocene north-
666 south extension in the high Himalaya revealed by Th-Pb monazite dating of the Khula
667 Kangri granite: Geology, v. 25, no. 6, p. 543-546.
668 Ferry, J. M., and Spear, F. S., 1978, Experimental calibration of the partitioning of Fe and Mg
669 between biotite and garnet: Contributions to Mineralogy and Petrology, v. 66-2, p. 113-
670 117.
671 Frank, W., Hoinkes, G., Miller, C., Purtscheller, F., Richter, W., and Thöni, M., 1973, Relations
672 between metamorphism and orogeny in a typical section of the Indian Himalayas:
673 Mineralogy and Petrology, v. 20, p. 303-332.
674 Gaetani, M., and Garzanti, E., 1991, Multicyclic history of the northern India continental margin
675 (Northwestern Himalaya): American Association of Petroleum Geologists Bulletin, v. 75,
676 p. 1427-1446.
677 Gansser, A., 1964, Geology of the Himalayas, Wiley Interscience, London, 289 p.
678 Gansser, A., 1983, Geology of the Bhutan Himalaya, Birkhauser Verlag, Basel, 181 p.

679 Gehrels, G., Kapp, P., DeCelles, P., Pullen, A., Blakey, R., Weislogel, A., Ding, L., Guynn, J.,
680 Martin, A., McQuarrie, N., and Yin, A., 2011, Detrital zircon geochronology of pre-
681 Tertiary strata in the Tibetan-Himalayan orogen: Tectonics, v. 30, no. TC5016, doi:
682 10.1029/2011TC002868.
683 Gehrels, G. E., DeCelles, P. G., Martin, A., Ojha, T. P., Pinhassi, G., and Upreti, B. N., 2003,
684 Initiation of the Himalayan orogen as an early Paleozoic thin-skinned thrust belt:
685 Geological Society of America Today, v. 13, no. 9, p. 4-9.
686 Ghent, E. D., and Stout, M. Z., 1981, Geobarometry and geothermometry of plagioclase-biotite-
687 garnet-muscovite assemblages: Contributions to Mineralogy and Petrology, v. 76-1, p.
688 92-97.
689 Gleeson, T. P., and Godin, L., 2006, The Chako antiform: a folded segment of the Greater
690 Himalayan sequence, Nar Valley, Central Nepal Himalaya: Journal of Asian Earth
691 Sciences, v. 27, p. 717-734.
692 Godin, L., Grujic, D., Law, R. D., and Searle, M. P., 2006, Crustal flow, extrusion, and
693 exhumation in continental collision zones: an introduction, *in* Law, R., Searle, M., and
694 Godin, L., eds., Channel Flow, Ductile Extrusion and Exhumation in Continental
695 Collision Zones, Volume 268, Geological Society London Special Publication, p. 1-28.
696 Grujic, D., Coutand, I., Bookhagen, B., Bonnet, S., Blythe, A., and Duncan, C., 2006, Climatic
697 forcing of erosion, landscape, and tectonics in the Bhutan Himalayas: Geology, v. 34, no.
698 10, p. 801-804.
699 Grujic, D., Hollister, L. S., and Parrish, R. R., 2002, Himalayan metamorphic sequence as an
700 orogenic channel: insight from Bhutan: Earth and Planetary Science Letters, v. 198, p.
701 177-191.

Grujic, D., Warren, C. J., and Wooden, J. L., 2011, Rapid synconvergent exhumation of Miocene-aged lower orogenic crust in the eastern Himalaya: Lithosphere, v. 3, no. 5, p. 346-366.

Guillot, S., Hodges, K. V., Le Fort, P., and Pêcher, A., 1994, New constraints on the age of the Manaslu leucogranite: Evidence for episodic tectonic denudation in the central Himalayas: Geology, v. 22, p. 559-562.

Guillot, S., Mahéo, G., de Sigoyer, J., Hattori, K. H., and Pêcher, A., 2008, Tethyan and Indian subduction viewed from the Himalayan high- to ultrahigh-pressure metamorphic rocks: Tectonophysics, v. 451, no. 1-4, p. 225-241.

Heim, A., and Gansser, A., 1939, Central Himalaya--Geological observations of Swiss expedition, 1936: Mémoire Société Helvétique Science Naturelle, v. 73, p. 1-245.

Herren, E., 1987, Zanskar shear zone; northeast-southwest extension within the Higher Himalayas (Ladakh, India): Geology, v. 15, p. 409-413.

Hodges, K., Bowring, S., Davidek, K., Hawkins, D., and Krol, M., 1998, Evidence for rapid displacement on Himalayan normal faults and the importance of tectonic denudation in the evolution of mountain ranges: Geology, v. 26, no. 6, p. 483-486.

Hodges, K., Hames, W., Olszewski, W., Burchfiel, B., Royden, L., and Chen, Z., 1994, Thermobarometric and $^{40}Ar/^{39}Ar$ geochronologic constraints on Eohimalayan metamorphism in the Dinggye area, southern Tibet: Contributions to Mineralogy and Petrology, v. 117, p. 151-163.

Hodges, K., Hurtado, J., and Whipple, K., 2001, Southward extrusion of Tibetan crust and its effect on Himalayan tectonics: Tectonics, v. 20, no. 6, p. 799-809.

Hodges, K., Parrish, R., Housh, T., Lux, D., Burchfiel, B., Royden, L., and Chen, Z., 1992, Simultaneous Miocene Extension and Shortening in the Himalayan Orogen: Science, v. 258, p. 1466-1470.

Hodges, K. V., 2000, Tectonics of the Himalaya and southern Tibet from two perspectives: Geological Society of America Bulletin, v. 112, no. 3, p. 324-350.

Hodges, K. V., Burchfiel, B. C., Royden, L. H., Chen, Z., and Liu, Y., 1993, The metamorphic signature of contemporaneous extension and shortening in the central Himalayan orogen: Data from the Nyalam transect, southern Tibet: Journal of Metamorphic Geology, v. 11, p. 721-737.

Hodges, K. V., Parrish, R. R., and Searle, M. P., 1996, Tectonic evolution of the central Annapurna Range, Nepalese Himalayas: Tectonics, v. 15, no. 6, p. 1264-1291.

Holland, T. J. B., and Powell, R., 1998, An internally consistent thermodynamic data set for phases of petrological interest: Journal of Metamorphic Geology, v. 16, p. 309-343.

Hollister, L. S., and Grujic, D., 2006, Pulsed channel flow in Bhutan, *in* Law, R., Searle, M., and Godin, L., eds., Channel Flow, Ductile Extrusion and Exhumation in Continental Collision Zones, Geological Society London Special Publication, p. 415-423.

Hubbard, M. S., and Harrison, T. M., 1989, $^{40}Ar/^{39}Ar$ age constraints on deformation and metamorphism in the Main Central thrust zone and Tibetan slab, eastern Nepal Himalaya: Tectonics, v. 8, p. 865-880.

Hughes, N. C., Myrow, P. M., McKenzie, N. R., Harper, D. A. T., Bhargava, O. N., Tangri, S. K., Ghalley, K. S., and Fanning, C. M., 2011, Cambrian rocks and faunas of the Wachi La, Black Mountains, Bhutan: Geological Magazine, v. 148, no. 3, p. 351-379.

746 Jangpangi, B. S., 1974, Stratigraphy and tectonics of parts of eastern Bhutan: Himalayan
747 Geology, v. 4, p. 139-147.
748 Katagiri, G., Ishida, H., and Ishitani, A., 1988, Raman spectra of graphite edge planes: Carbon,
749 v. 26, no. 4, p. 565--571.
750 Kellett, D., Grujic, D., and Erdmann, S., 2009, Miocene structural reorganization of the South
751 Tibetan detachment, eastern Himalaya: Implications for continental collision:
752 Lithosphere, v. 1, no. 5, p. 259-281.
753 Kellett, D., Grujic, D., Warren, C., Cottle, J., Jamieson, R., and Tenzin, T., 2010, Metamorphic
754 history of a syn−convergent orogen−parallel detachment: The South Tibetan detachment
755 system, Bhutan Himalaya: Journal of Metamorphic Geology.
756 Kellett, D. A., and Grujic, D., 2012, New insight into the South Tibetan detachment system: Not
757 a single progressive deformation: Tectonics, v. 31, no. TC2007, doi:
758 10.1029/2011TC002957.
759 Large, D. J., Christy, A. G., and Fallick, A. E., 1994, Poorly crystalline carbonaceous matter in
760 high grade metasediments: implications of graphitization and metamorphic fluids
761 compositions: Contributions to Mineralogy and Petrology, v. 116, p. 108-116.
762 Law, R., Searle, M., and Godin, L., 2006, Channel Flow, Ductile Extrusion and Exhumation in
763 Continental Collision Zones, Geological Society London Special Publication, 632 p.
764 Law, R. D., Jessup, M. J., Searle, M. P., Francsis, M. K., Waters, D. J., and Cottle, J. M., 2011,
765 Telescoping of isotherms beneath the South Tibetan Detachment System, Mount Everest
766 Massif: Journal of Structural Geology, v. 33, p. 1569-1594, doi:
767 10.1016/j.jsg.2011.09.004.

768 Le Fort, P., 1975, Himalayas: The collided range. Present knowledge of the continental arc:
769 American Journal of Science, v. 275-A, p. 1-44.
770 Leech, M. L., Singh, S., Jain, A. K., Klemperer, S. L., and Manickavasagam, R. M., 2005, The
771 onset of India-Asia continental collision: Early, steep subduction required by the timing
772 of UHP metamorphism in the western Himalaya: Earth and Planetary Science Letters, v.
773 234, p. 83-97.
774 Lister, G. S., and Snoke, A. W., 1984, S-C mylonites: Journal of Structural Geology, v. 6, p. 617-
775 638.
776 Lombardo, B., Pertusati, P., and Borghi, S., 1993, Geology and tectonomagmatic evolution of
777 the eastern Himalaya along the Chomolungma-Makalu transect, *in* Treloar, P. J., and
778 Searle, M. P., eds., Himalayan Tectonics, Volume 74, Geological Society Special
779 Publication, p. 341-355.
780 Long, S., and McQuarrie, N., 2010, Placing limits on channel flow: Insights from the Bhutan
781 Himalaya: Earth and Planetary Science Letters, v. 290, p. 375-390.
782 Long, S., McQuarrie, N., Tobgay, T., and Grujic, D., 2011a, Geometry and crustal shortening of
783 the Himalayan fold-thrust belt, eastern and central Bhutan: Geological Society of
784 America Bulletin, doi: 10.1130/B30203.1.
785 Long, S., McQuarrie, N., Tobgay, T., Rose, C., Gehrels, G., and Grujic, D., 2011b,
786 Tectonostratigraphy of the Lesser Himalaya of Bhutan: Implications for the along-strike
787 stratigraphic continuity of the northern Indian margin: Geological Society of America
788 Bulletin.
789 Long, S. P., McQuarrie, N., Tobgay, T., Grujic, D., and Hollister, L., 2011c, Geologic map of
790 Bhutan: The Journal of Maps, v. 2011, p. 184-192, doi: 10.4113/jom.2011.1159.

McQuarrie, N., Robinson, D., Long, S., Tobgay, T., Grujic, D., Gehrels, G., and Ducea, M., 2008, Preliminary stratigraphic and structural architecture of Bhutan: Implications for the along strike architecture of the Himalayan system: Earth and Planetary Science Letters, v. 272, p. 105-117, doi: 10.1016/j.epsl.2008.04.030.

Mu, A. T., Wen, S. H., Wang, Y. K., Chang, P. K., and Yin, C. H., 1973, Stratigraphy of the Mount Jolmo Lungma region in Southern Tibet, China: Scientia Sinica, v. 16, p. 96-111.

Myrow, P. M., Hughes, N. C., Searle, M. P., Fanning, C. M., Peng, S.-C., and Parcha, S. K., 2009, Stratigraphic correlation of Cambrian-Ordovician deposits along the Himalaya: Implications for the age and nature of rocks in the Mount Everest region: Geological Society of America Bulletin, v. 120, no. 3/4, p. 323-332, doi: 10.1130/B26384.1.

Najman, Y., Clift, P., Johnson, M. R. W., and Robertson, A. H. F., 1993, Early stages of foreland basin evolution in the Lesser Himalaya, N India, *in* Treloar, P. J., and Searle, M. P., eds., Himalayan tectonics, Volume 74, Geological Society of London Special Publication p. 541-558.

Najman, Y. M. R., Pringle, M. S., Johnson, M. R. W., A.H.F., R., and Wijbrans, J. R., 1997, Laser $^{40}Ar/^{39}Ar$ dating of single detrital muscovite grains from early foreland basin deposits in India: Implications for early Himalayan evolution: Geological Society of America Special Paper, v. 232, p. 243-264.

Nautiyal, S. P., Jangpangi, B. S., Singh, P., Guha Sarkar, T. K., Bhate, V. D., Raghavan, M. R., and Sahai, T. N., 1964, A preliminary note on the geology of the Bhutan Himalaya: Report of the 22nd International Geologic Congress, New Delhi, v. 11, p. 1-14.

Nelson, K. D., Zhao, W., Brown, L. D., Kuo, J., Che, J., Xianwen, L., Klemperer, S., Makovsky, Y., Meissner, R., Mechie, J., Kind, R., Wenzel, F., Ni, J., Nabelek, J., Chen, L., Handong,

814 T., Wenbo, W., Jones, A. G., Booker, J., Unsworth, M., Kidd, W. S. F., Hauk, M.,
815 Alsdorf, D., Ross, A., Cogan, M., Wu, C., Sandvol, E. A., and Edwards, M., 1996,
816 Partially molten middle crust beneath southern Tibet: Synthesis of Project INDEPTH
817 Results: Science, v. 274, p. 1684-1688.
818 Parrish, R. R., and Hodges, K. V., 1996, Isotopic constraints on the age and provenance of the
819 Lesser and Greater Himalayan sequences, Nepalese Himalaya: Geological Society of
820 America Bulletin, v. 108, p. 904-911.
821 Pêcher, A., 1991, The contact between the higher Himalaya crystallines and the Tibetan
822 sedimentary series: Miocene large-scale dextral shearing: Tectonics, v. 10, no. 3, p. 587-
823 598.
824 Pognante, U., and Benna, P., 1993, Dynamics of orogenic wedges and the uplift of high-pressure
825 metamorphic rocks: Geological Society of London Special Publication, v. 74, p. 323-340.
826 Powell, R., and Holland, T. J. B., 1988, An internally consistent dataset with uncertainties and
827 correlations: 3. Applications to geobarometry, worked examples and a computer
828 program: Journal of Metamorphic Geology, v. 6, p. 173-204.
829 Rahl, J. M., Anderson, K. M., Brandon, M. T., and Fassoulas, C., 2005, Raman spectroscopic
830 carbonaceous material thermometry of low-grade metamorphic rocks: Calibration and
831 application to tectonic exhumation in Crete, Greece: Earth and Planetary Science Letters,
832 v. 240, p. 339-354.
833 Rietmeijer, F. J. M., and Mackinnon, I. D. R., 1985, Poorly graphitized carbon as a new
834 cosmothermometer for primitive extraterrestrial materials: Nature, v. 316, p. 733-736.

835 Robinson, D. M., DeCelles, P. G., and Copeland, P., 2006, Tectonic evolution of the Himalayan
836 thrust belt in western Nepal: implications for channel flow models: Geological Society of
837 America Bulletin, v. 118, p. 865-885.
838 Rowley, D. B., 1996, Age of initiation of collision between India and Asia: A review of
839 stratigraphic data: Earth and Planetary Science Letters, v. 145, p. 1-13.
840 Searle, M., and Godin, L., 2003, The South Tibetan Detachment and the Manaslu Leucogranite:
841 A Structural Reinterpretation and Restoration of the Annapurna-Manaslu Himalaya,
842 Nepal: The Journal of Geology, v. 111, p. 505-523.
843 Searle, M., Parrish, R., Hodges, K., Hurford, A., Ayers, M., and Whitehouse, M., 1997, Shisha
844 Pangma leucogranite, South Tibetan Himalaya: Field relations, geochemistry, age, origin,
845 and emplacement: Journal of Geology, v. 105, p. 295-317.
846 Searle, M., Simpson, R., Law, R., Parrish, R., and Waters, D., 2003, The structural geometry,
847 metamorphic and magmatic evolution of the Everest massif, High Himalaya of Nepal-
848 South Tibet: Journal of the Geological Society, v. 160, p. 345-366.
849 Searle, M., Simpson, R., Law, R., Waters, D., and Parrish, R., 2002, Quantifying displacement
850 on the South Tibetan Detachment normal fault, Everest massif, and the timing of crustal
851 thickening and uplift in the Himalaya and Tibet: Journal of Nepal Geological Society, v.
852 26, p. 1-6.
853 Searle, M. P., 1986, Structural evolution and sequence of thrusting in the High Himalayan,
854 Tibetan-Tethys and Indus suture zones of Zanskar and Ladakh, western Himalaya:
855 Journal of Structural Geology, v. 8, p. 923-936.
856 Searle, M. P., 1999, Extensional and compressional faults in the Everest-Lhotse Massif, Khumbu
857 Himalaya, Nepal: Journal of the Geological Society, London, v. 156, p. 227-240.

858 Searle, M. P., Law, R. D., and Jessup, M. J., 2006, Crustal structure, restoration and evolution of
859 the Greater Himalaya in Nepal--South Tibet: implications for channel flow and ductile
860 extrusion of the middle crust, *in* Law, R., Searle, M., and Godin, L., eds., Channel Flow,
861 Ductile Extrusion and Exhumation in Continental Collision Zones, Volume 268,
862 Geological Society London Special Publication, p. 355-378.
863 Searle, M. P., and Rex, A. J., 1989, Thermal model for the Zanskar Himalaya: Journal of
864 Metamorphic Geology, v. 7, p. 127-134.
865 Singh, S. K., Trivedi, J. R., and Krishnaswami, S., 1999, Re-Os isotope systematics in black
866 shales from the Lesser Himalaya: Their chronology and role in the $^{187}Os/^{188}Os$ evolution
867 of seawater: Geochimica et Cosmochimica Acta, v. 63, p. 2381-2392.
868 Stöcklin, J., 1980, Geology of Nepal and its regional frame: Journal of the Geological Society,
869 London, v. 137, p. 1-34.
870 Stüwe, K., and Foster, D., 2001, 40Ar/39Ar, pressure, temperature and fission track constraints
871 on the age and nature of metamorphism around the main central thrust in the eastern
872 Bhutan Himalaya: Journal of Asian Earth Sciences, v. 19, p. 85-95.
873 Swapp, S. M., and Hollister, L. S., 1991, Inverted metamorphism within the Tibetan slab of
874 Bhutan; evidence for a tectonically transported heat-source: Canadian Mineralogist, v.
875 29, p. 1019-1041.
876 Tangri, S. K., and Pande, A. C., 1995, Tethyan Sequence, *in* Bhargava, O. N., ed., The Bhutan
877 Himalaya: a geological account: Calcutta, Geological Survey of India, p. 109-141.
878 Tobgay, T., McQuarrie, N., Long, S., Kohn, M. J., and Corrie, S. L., 2012, The age and rate of
879 displacement along the Main Central Thrust in the western Bhutan Himalaya: Earth and
880 Planetary Science Letters, v. 319-320, p. 146-158.

881 Valdiya, K. S., 1980, Geology of the Kumaun Lesser Himalaya, Dehra Dun, Wadia Institute of
882 Himalayan Geology.
883 Valdiya, K. S., 1989, Trans-Himadri intracrustal fault and basement upwarps south of the Indus-
884 Tsangpo suture zone, *in* Malinconico, L., and Lillie, R., eds., Tectonics of the western
885 Himalayas, Volume 232, Geological Society of America Special Paper, p. 153-168.
886 Vannay, J.-C., and Hodges, K., 1996, Tectonometamorphic evolution of the Himalayan
887 metamorphic core between the Annapurna and Dhaulagiri, central Nepal: Journal of
888 Metamorphic Geology, v. 14, p. 635-656.
889 Walker, J. D., Martin, M. W., Bowring, S. A., Searle, M. P., Waters, D. J., and Hodges, K. V.,
890 1999, Metamorphism, melting, and extension: age constraints from the High Himalayan
891 slab of southeast Zanskar and northwest Lahaul: Journal of Geology, v. 107, p. 473-495.
892 Wang, Z., and Zhen, X., 1975, Imbricate structure in the northern slope of Jolmo Lungma and
893 discussion of the uplift of the Himalaya, Scientific exploration of Jolmo Lungma:
894 Beijing, Science Publishing House, p. 199-221.
895 Wopenka, B., and Pasteris, J. D., 1993, Structural characterization of kerogens to granulite facies
896 graphite; applicability of Raman microprobe spectroscopy: American Mineralogist, v. 78,
897 p. 533-557.
898 Wu, C., Nelson, K. D., Wortman, G., Samson, S. D., Yue, Y., Li, J., Kidd, W. S. F., and
899 Edwards, M. A., 1998, Yadong cross structure and South Tibetan Detachment in the east
900 central Himalaya (89-90ºE): Tectonics, v. 17, no. 1, p. 28-45.
901 Yin, A., 2006, Cenozoic tectonic evolution of the Himalayan orogen as constrained by along-
902 strike variation of structural geometry, exhumation history, and foreland sedimentation:
903 Earth Science Reviews, v. 76, p. 1-131.

Yin, A., Dubey, C. S., Kelty, T. K., Webb, A. A. G., Harrison, T. M., Chou, C. Y., and Celerier, J., 2010, Geologic correlation of the Himalayan orogen and Indian craton: Part 2. Structural geology, geochronology, and tectonic evolution of the Eastern Himalaya: Geological Society of America Bulletin, v. 122, no. 3/4, p. 360-395.

Yin, A., Harrison, T. M., Ryerson, F. J., Chen, W., Kidd, W. S. F., and Copeland, P., 1994, Tertiary structural evolution of the Gangdese thrust system, southeastern Tibet: Journal of Geophysical Research, v. 99, p. 18175-18201.

FIGURE CAPTIONS

Figure 1. Simplified geologic map of Bhutan and surrounding regions. Compiled from Gansser (1983), Bhargava (1995), Grujic et al. (2002), Long and McQuarrie (2010), Long et al. (2011c), Hughes et al. (2011), and Cooper et al. (in press). Box indicates the location of the study area shown in Figure 3. Inset map: A simplified tectonic map of the Himalayan orogen (modified from Hodges (2000) and Long et al. (2011c)). Abbreviations: STFS = South Tibetan fault system; KT = Kakhtang thrust; MCTS = Main Central thrust system; MBTS = Main Boundary thrust system; MFTS = Main Frontal thrust system; PW = Paro window; YCS = Yadong cross structure; Jo = Mount Jomolhari; KK = Khula Kangri pluton; WL = Wagye La; GL = Gonto La; LLK = Lhozhag La Kang; DCK = Dang Chu (Tang Chu) klippe; UK = Ura klippe; ZK = Zhemgang (Black Mountain) klippe; SK = Sakteng (Radi) klippe. Interpreted contacts at the base of the Dang Chu, Ura, and Zhemgang klippen follow Long and McQuarrie (2010). Cross-section line A–A' refers to Figures 3 and 9.

Figure 2. Alternative geologic interpretations of central Bhutan. (a) Long and McQuarrie (2010) interpret the Dang Chu and Ura klippen as being soled by the STFS but map the GHS-Chekha contact at the base of the Zhemgang klippe as a conformable contact. The breakaway zone for the STFS is inferred to lie between the two klippen. (b) Grujic et al. (2011) map the Chekha Formation more extensively across central Bhutan, joining the Dang Chu and Zhemgang klippen and extending the Ura klippe northward, where it is cut by the Kakhtang Thrust. RSCM sampling locations for this study and the location of Cambrian fossils found by Hughes et al. (2011) are shown. The RSCM results are split into three groups according to peak metamorphic temperature. Abbreviations follow Figure 1. Stars refer to outcrop photographs in Figure 4.

Figure 3. Schematic cross-sections for the contrasting geological interpretations of (a) Long and McQuarrie (2010) and (b) Grujic et al. (2011). In (a), the distance between the STFS breakaway zone and the Ura klippe to the north implies a maximum displacement on the STFS of ca. 20 km. In (b), the distance from the STFS exposed at the crest of the range to the southernmost extent of the Zhemgang klippe implies a minimum displacement of 100 km on the STFS.

Figure 4. Outcrops of Tibetan Sedimentary sequence, Chekha Formation, and Greater Himalayan sequence units illustrating differences in structural style. Locations are shown in Figure 2. (a) and (b) Large-scale recumbent folding in TSS marbles of the Dang Chu klippe, (a) next to the Baylangdra monastery, and (b) at Pele La. (c) A cliff of Chekha Formation quartzite in the Dang Chu klippe dips consistently to the north and shows no evidence for large scale folding. This fundamental change in structural style is the same as the change across the STFS mapped by Cooper et al. (in press) in the Jomolhari area of NW Bhutan. (d) GHS pelitic schists

949 north of the Ura klippe show a similar consistently north-dipping fabric, with no large-scale
950 folding. (e) Chekha Formation quartzites and (f) interbedded quartzite and phyllite of the TSS
951 Maneting formation (as mapped by Long et al. (2011c) in the Zhemgang klippe dips gently to the
952 south and also shows no evidence for large-scale folding.
953
954 **Figure 5.** Simplified stratigraphic columns for central Bhutan showing how different research
955 groups have interpreted the stratigraphy and positions of the major fault systems. For
956 abbreviations, see Figure 1. Age ranges follow Hughes et al. (2011); Long and McQuarrie
957 (2010); and Tangri and Pande (1995). Unit thicknesses (shown in kilometers on the right hand
958 side of each column) are from Long and McQuarrie (2010); Long et al. (2011a); and Tangri and
959 Pande (1995).
960
961 **Figure 6.** Examples of Raman spectra for each sample. The positions of the graphite band, G,
962 and defect bands D1 and D2 are indicated. R2 values and temperatures calculated using the
963 Beyssac et al. (2002a) calibration are given. Full details of peak positions for individual analyses
964 are given in Data Repository Item B.
965
966 **Figure 7.** All 17 samples plotted in order of peak metamorphic temperature. 13 samples (FB52
967 to FB102) show very consistent temperatures, with an error-weighted mean average of 560 ±
968 2°C (2SE). These samples include TSS marbles and phyllites (Maneting Formation), Chekha
969 Formation schists, quartzites, and calc-silicates as well as GHS paragneisses and schists across
970 all three klippen (Figure 2). The lack of any temperature difference between the Chekha, GHS,
971 and TSS Maneting Formation samples suggests that there is no metamorphic discontinuity across

between them. Four samples give distinctly lower temperatures: Samples FB64 and FB85, both foliated calc-silicates, give temperatures of 508 ± 33°C and 489 ± 26°C (2SE), respectively, while samples FB28, a marble and FB77, a black shale give 430 ± 30°C and 420 ± 21°C, respectively.

Figure 8. Our interpretation for the distribution of RSCM temperatures in central Bhutan. Abbreviations: DCKn = Dang Chu klippe, north; DCKs = Dang Chu klippe, south; STFS = South Tibetan fault system; KT = Kakhtang thrust; MCTS = Main Central thrust system; MBTS = Main Boundary thrust system. (a) The Chekha Formation and GHS are combined as one sequence due to their similar lithology, structural style and peak metamorphic temperature. The TSS in the Dang Chu klippe is mapped on the basis of the four lower-temperature samples, FB28, FB64, FB77 and FB85 as well as our structural observations of recumbently folded units and the location of fossils found by Hughes et al. (2011). We interpret the contact between the TSS and structurally lower units to be the sole STFS detachment. (b) Schematic cross-section through the north and south components of the Dang Chu klippe. The distance from the STFS exposed at the crest of the range to the southernmost extent of the Dang Chu klippe implies a minimum displacement of 80 km on the STFS.

[1]GSA Data Repository item 2012xxx, Examples of analyzed carbonaceous material, complete RSCM spectra data, and thermobarometric methods and data tables, is available online at www.geosociety.org/pubs/ft2009.htm, or on request from editing@geosociety.org or Documents Secretary, GSA, P.O. Box 9140, Boulder, CO 80301, USA.

Cooper et al. Figure 1

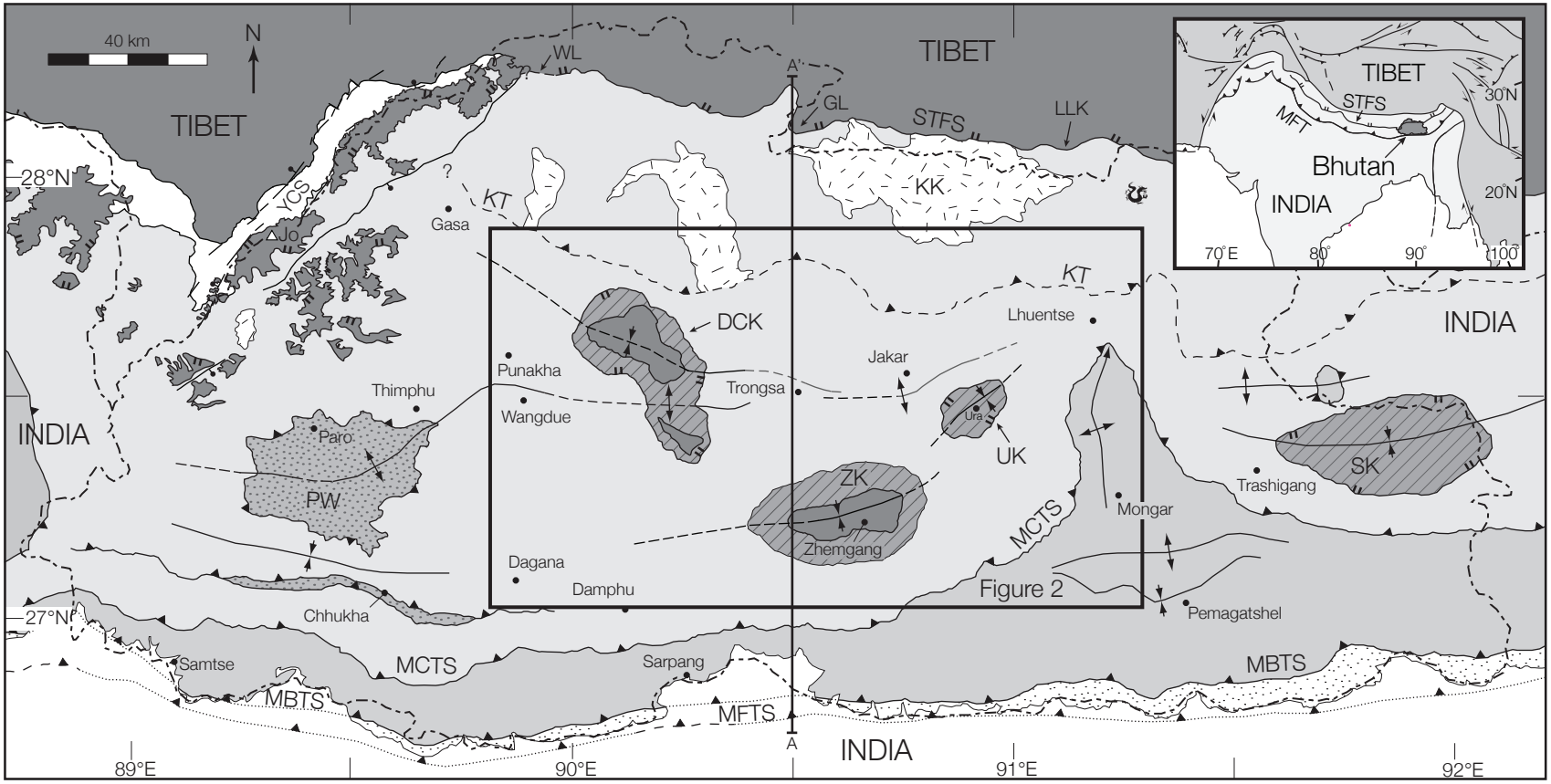

Tibetan Sedimentary sequence (TSS) (undifferentiated)

Chekha Formation

Leucogranites

Greater Himalayan sequence (GHS) (undifferentiated)

Paro Formation

Lesser Himalayan sequence (LHS) (undifferentiated)

Subhimalaya (Siwalik Group)

Quaternary sediment

South Tibetan fault system (STFS)

Thrust fault system

High-angle normal fault

Syncline; anticline

International border

Dragons

Cooper et al. Figure 2

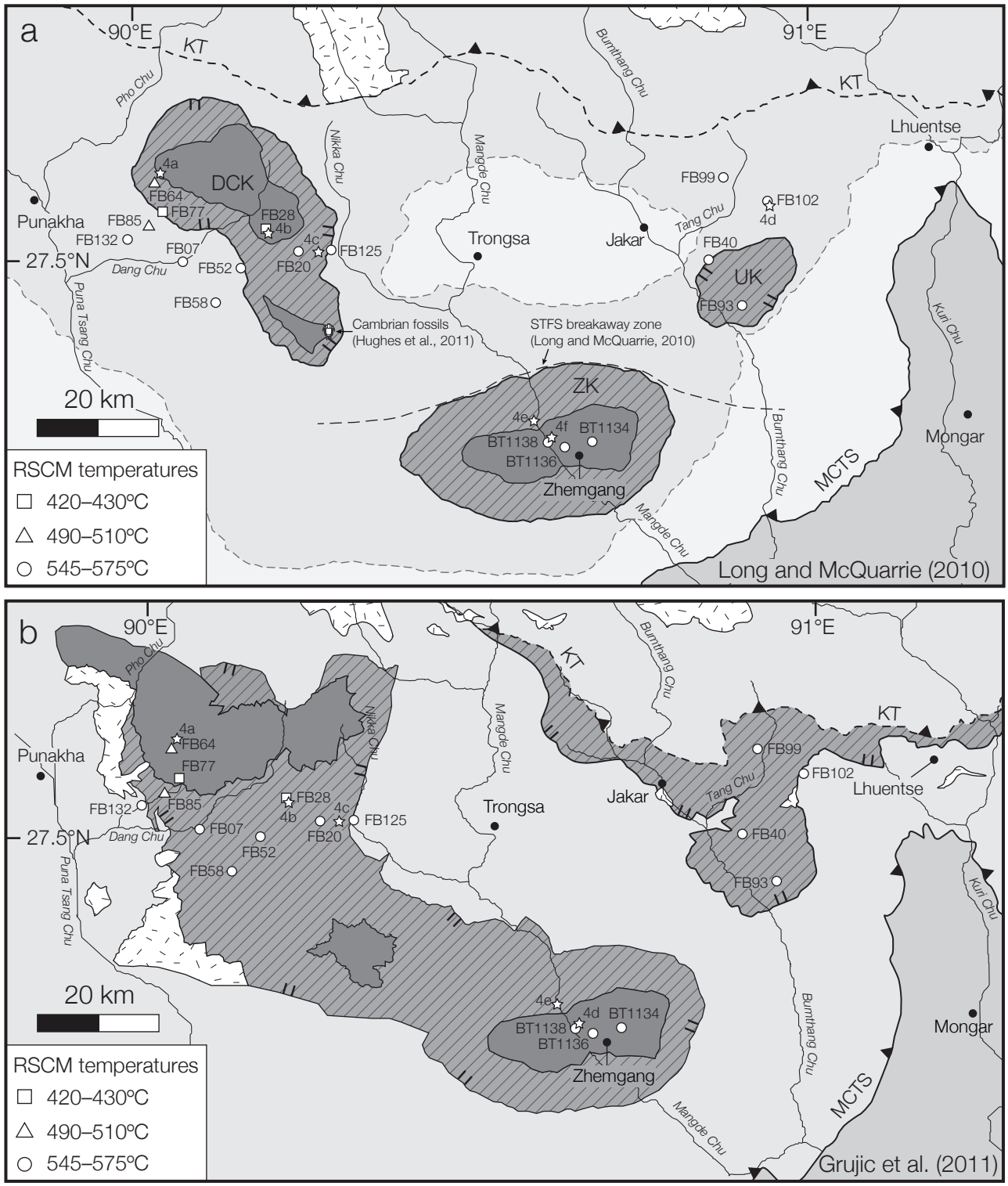

Cooper et al. Figure 3

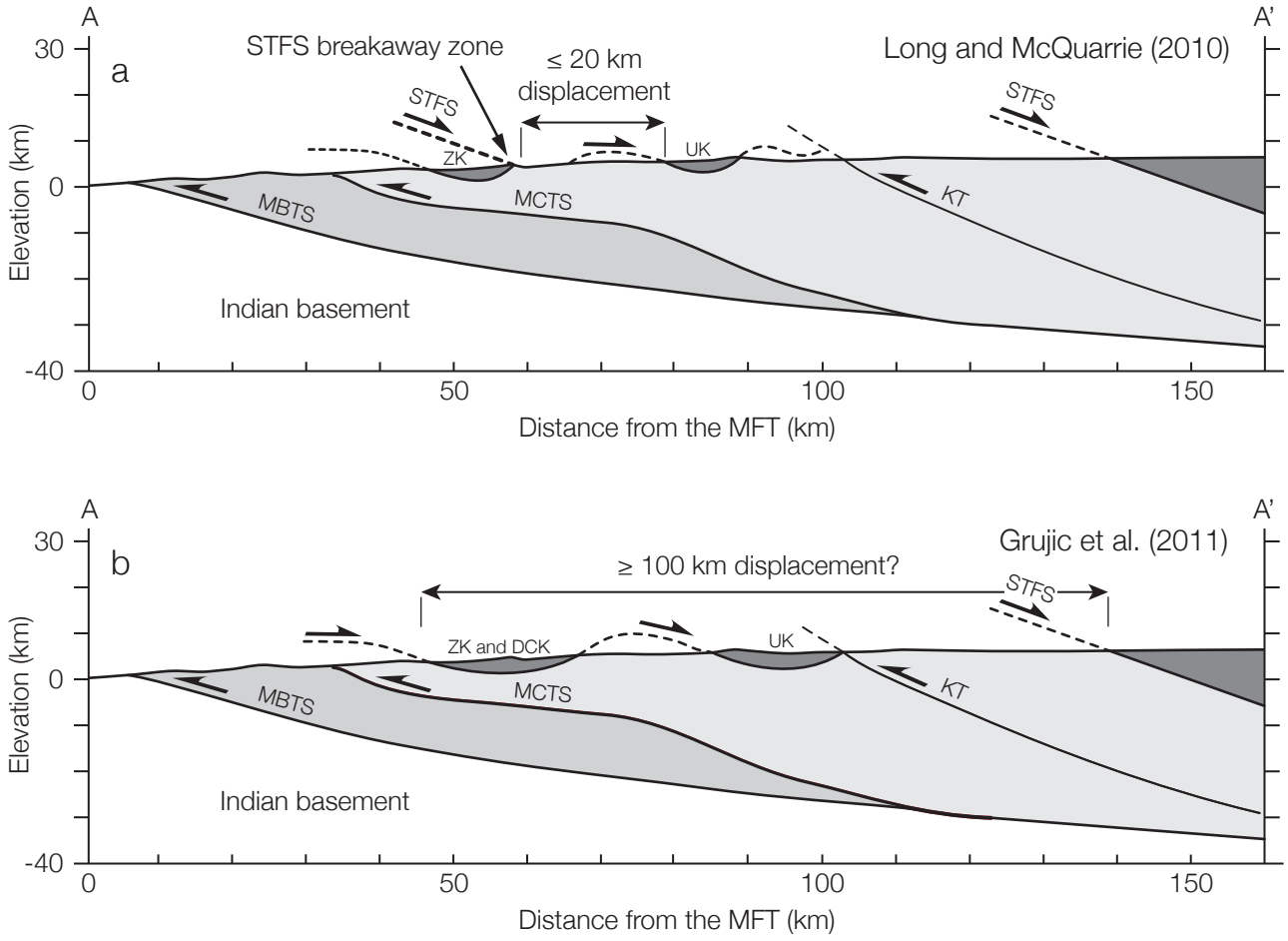

Cooper et al. Figure 4

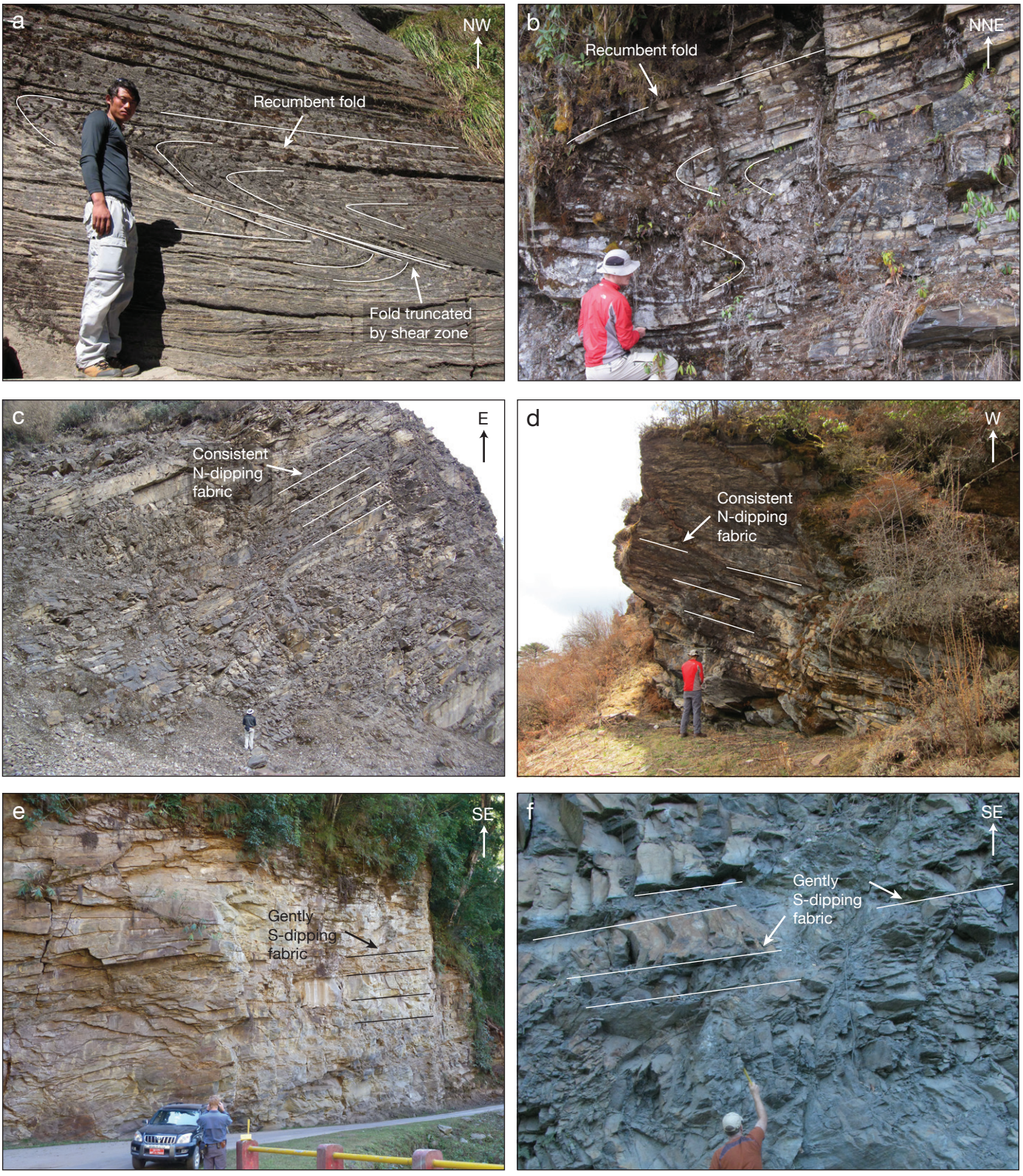

Cooper et al. Figure 5

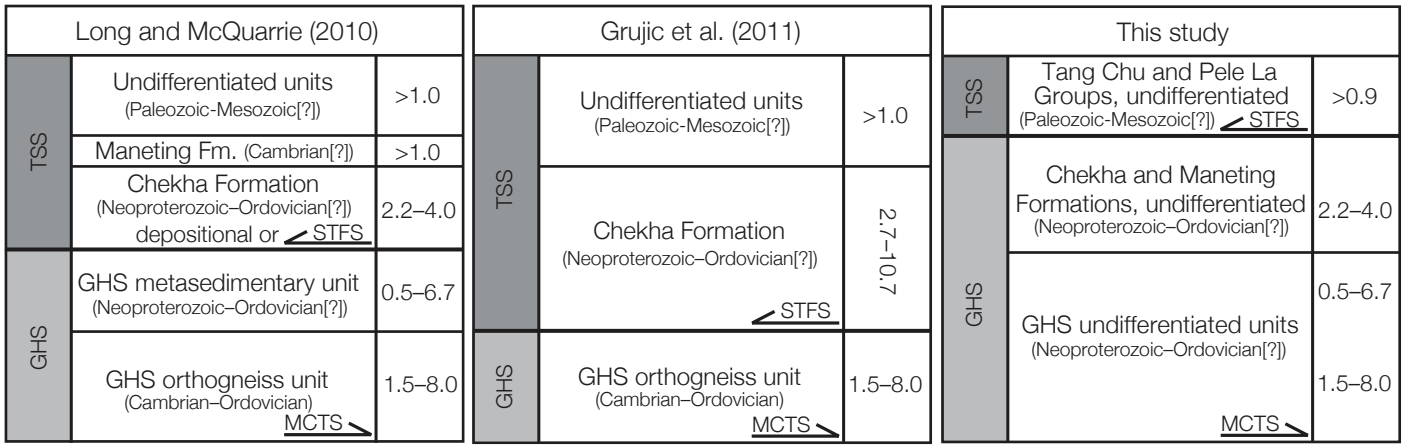

Cooper et al. Figure 6

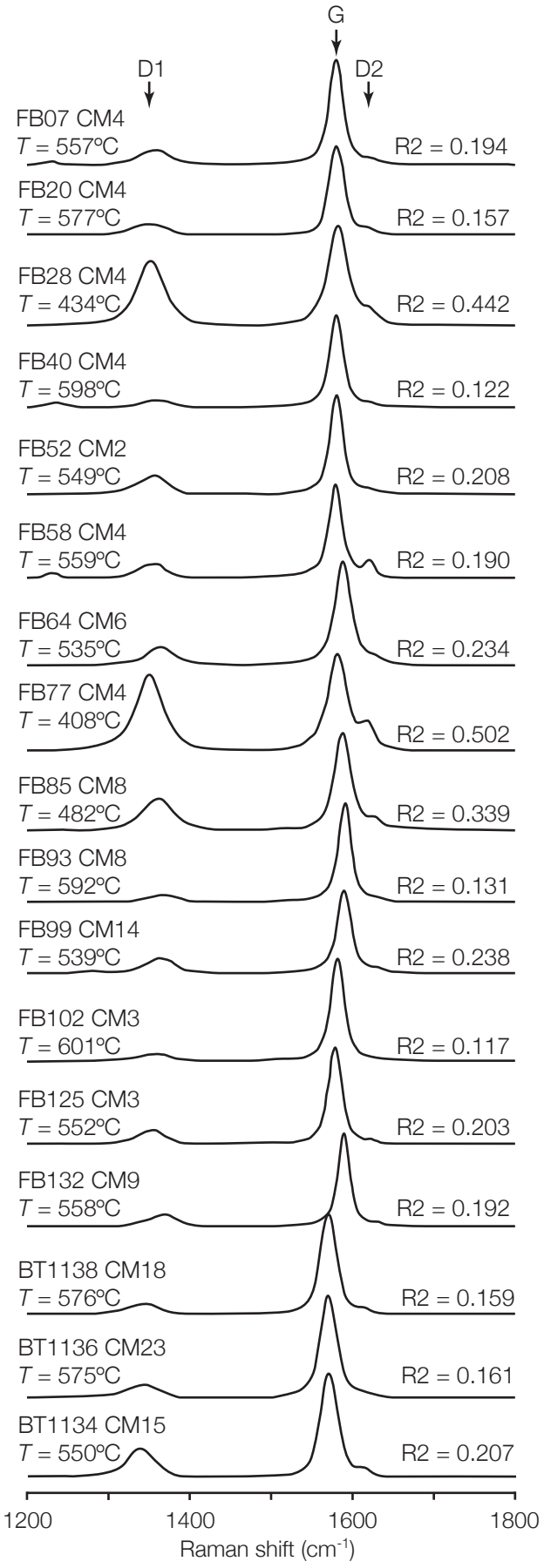

Cooper et al. Figure 7

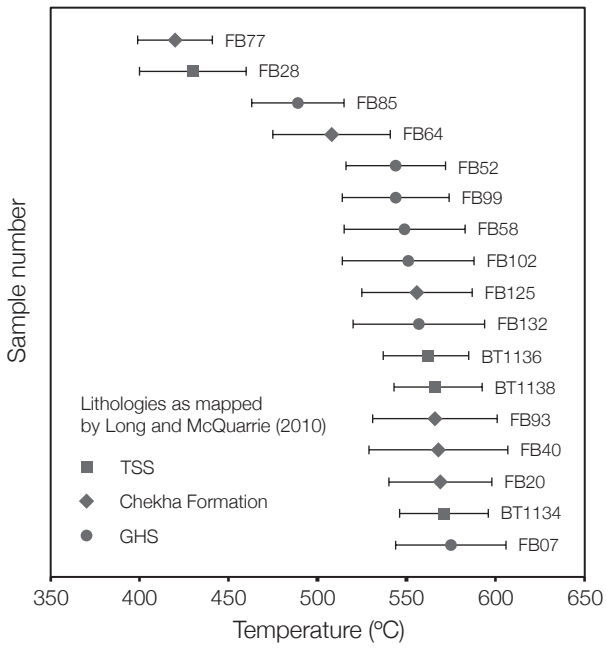

Cooper et al. Figure 8

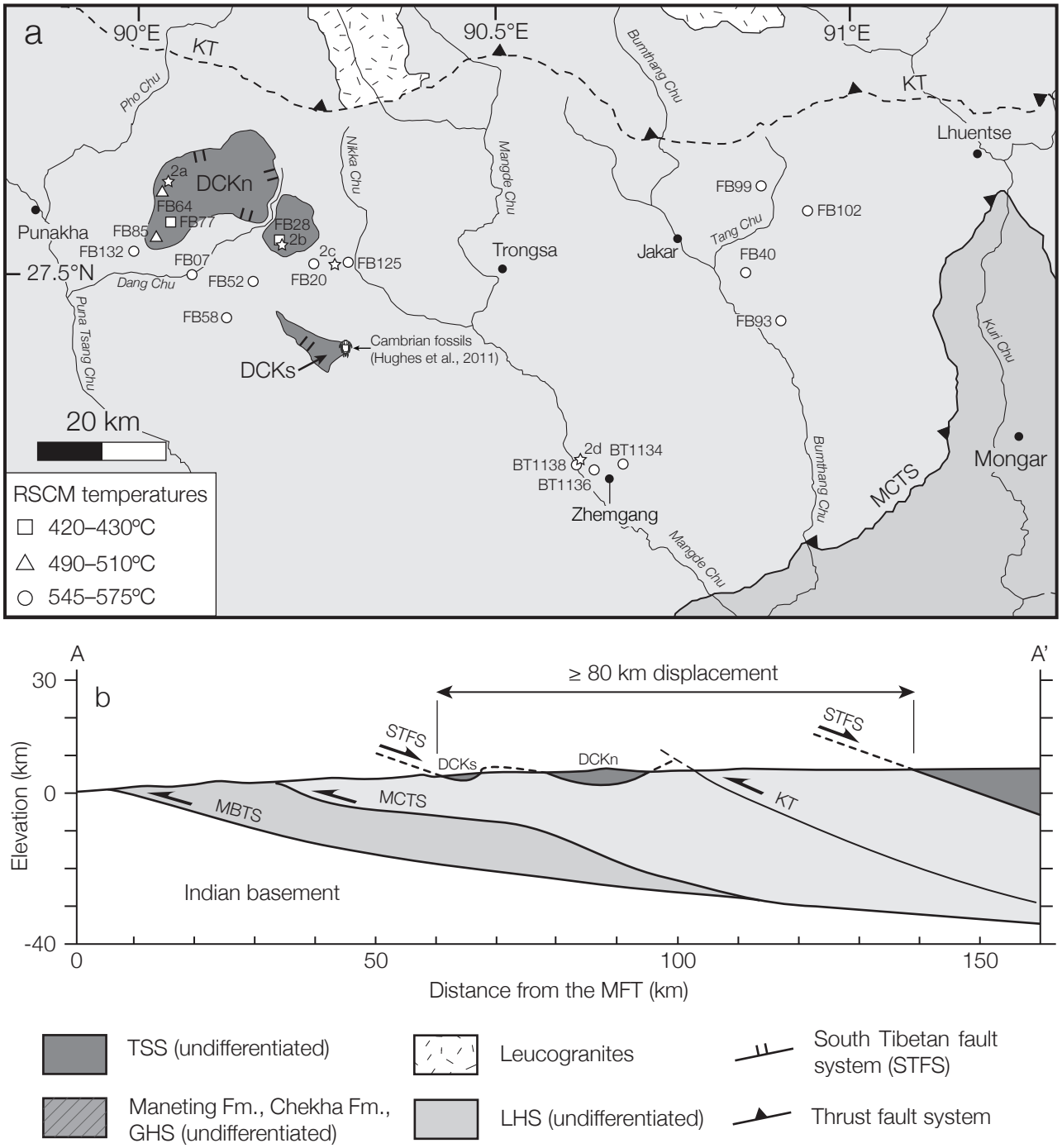

Table 1. RSCM temperatures

Sample	Lithology	Location		R2		Temp (°C)			n
		Latitude (°)	Longitude (°)	Mean	1σ	Mean	1σ	2SE	
FB07	Paragneiss	27.505	90.078	0.165	0.090	575	49	31	20
FB20	Quartzite	27.518	90.250	0.175	0.071	569	40	29	20
FB28	Marble	27.551	90.202	0.454	0.073	430	31	30	15
FB40	Paragneiss	27.504	90.854	0.178	0.104	568	57	39	15
FB52	Pelitic schist	27.496	90.165	0.220	0.073	544	39	28	20
FB58	Quartzite	27.445	90.127	0.212	0.080	549	43	34	15
FB64	Calc-silicate	27.617	90.036	0.288	0.082	508	40	33	15
FB77	Graphitic slate	27.577	90.048	0.474	0.038	420	16	21	25
FB85	Calc-silicate	27.556	90.028	0.326	0.061	489	31	26	20
FB93	Pelitic schist	27.436	90.905	0.169	0.105	566	47	35	15
FB99	Marble	27.625	90.876	0.220	0.083	544	46	30	20
FB102	Paragneiss	27.591	90.941	0.209	0.098	551	52	37	15
FB125	Paragneiss	27.520	90.299	0.200	0.098	556	53	31	22
FB132	Paragneiss	27.537	89.997	0.200	0.122	557	66	37	20
BT1134	Phyllite	27.236	90.681	0.171	0.070	571	39	25	25
BT1136	Phyllite	27.228	90.638	0.189	0.060	561	33	24	25
BT1138	Phyllite	27.234	90.615	0.179	0.055	566	31	23	25

R2 values calculated using the calibration of Beyssac et al. (2002a) and temperatures calculated using Aoya (2010). Variability of the R2 value within each sample is indicated by its 1σ uncertainty.

Temperatures are reported as standard means at the 1σ and 2 standard errors (2SE) confidence levels, accounting for both internal and external uncertainties (see also Data Repository Item B).

Table 2. RSCM vs GARB-GMBP results

Sample	RSCM[a] Temp (°C)			GARB[b] Temp (°C)		GMBP[b] Pressure (kbar)		
	Mean	2SE	n	Mean	2SE	Mean	2SE	n
FB07	575	31	20	579	48	5.0	0.6	3
FB125	556	31	22	532	56	6.2	0.8	4
FB132	557	37	20	536	75	4.5	0.8	3

[a]RSCM temperatures were calculated using the Aoya (2010) calibration. [b]GARB temperatures and GMBP pressures were calculated using THERMOCALC v. 3.33. All data are reported as means at the 2 standard errors confidence level.